DESIGN OF SPECTRALLY SELECTIVE COATINGS FOR HIGH EFFICIENCY POWER GENERATION DEVICES

by

Farhad Kazemi Khosroshahi

B.S., Mechanical Engineering, Azad University of Tabriz, 2006

M.S., Energy Conversion, Azad University of Tabriz, 2010

Submitted to the Institute for Graduate Studies in
Science and Engineering in partial fulfillment of
the requirements for the degree of
Doctor of Philosophy

Graduate Program in Mechanical Engineering

Boğaziçi University

2017

DESIGN OF SPECTRALLY SELECTIVE COATINGS FOR HIGH EFFICIENCY POWER GENERATION DEVICES

APPROVED BY:

Assoc. Prof. Hakan Ertürk ..... (Thesis Supervisor)

Prof. M. Pınar Mengüç ..... (Thesis Co-supervisor)

Assoc. Prof. Hasan Bedir .....

Assist. Prof. Nazlı Dönmezer .....

Prof. Kurşat Şendur .....

DATE OF APPROVAL: DD.MM.YYYY

ACKNOWLEDGEMENTS

First and foremost I want to thank my supervisor Assoc. Prof. Hakan Ertürk. It has been an honor to be his first Ph.D. student. He has been supportive since the days I began working. My Ph.D. thesis and related achievement would not be possible without his valuable advices and encouragements.

The thesis would not have come to a successful completion, without the help I received from my co-supervisor Prof. M. Pınar Mengüç. His scientific point of views shaped the major portion of the thesis.

I would like to express my sincere gratitude to my thesis committee, Assoc. Prof. Hasan Bedir, Assist. Prof. Nazlı Dönmezer, Prof. Kurşat Şendur, and Assist. Prof. Sedat Nizamoğlu for their precious recommendations.

At last, but definitely not the least, I want to thank to my family. My father, Mohammadreza and my mother Parvin, who raised me with a love of science and supported me in all my pursuits. To my little and cute nephew and niece, Aria and Tania. Having them, although far away, motivated me to confront with numerous challenges.

The author also gratefully acknowledges the fellowship provided by the Scientific and Technological Research Council of Turkey (TUBITAK) under the BIDEB-2215 program.

ABSTRACT

DESIGN OF SPECTRALLY SELECTIVE COATINGS FOR HIGH EFFICIENCY POWER GENERATION DEVICES

This thesis is aimed at designing and optimizing spectrally selective emitters/ filters for optical or thermal applications such as thermophotovoltaic (TPV) devices. Using spectrally selective emitters/filters in these devices is a crucial step to approach to an optimum system. Design of a spectrally selective filter based on one-dimensional Si/SiO_2 layers is considered first for improved performance of TPV devices. Spectrally selective filters transmit only the convertible radiation from the emitter as non-convertible radiation leads to a reduction in cell efficiency due to heating. The presented Si/SiO_2 based filter concept reflects the major part of the unconvertible range back to the emitter to minimize energy required for the process and it is adaptable to different types of cells and emitters with different temperatures since its cut-off wavelength can be tuned. While this study mainly focuses on InGaSb based TPV cell, Si, GaSb, and $Ga_{0.78}In_{0.22}As_{0.19}Sb_{0.81}$ based cells are also examined. The simulations show that significant enhancement in the overall system and device efficiency is possible by using such filters with TPV devices. In addition, graphene based spectrally selective nano-structures are theoretically investigated to achieve absorption and transmission within narrow wavelength bands. Two concepts are identified to control the spectral absorptance and transmittance and the results showed that using these two-dimensional, multi-layered structures, with gratings and graphene layers narrow-band absorptance and transmittance can be achieved. The effect of the graphene layer is identified for the emitter structure using power dissipation profiles. The suggested filter structure is then optimized for a TPV system and it is shown that the overall TPV system efficiency can be improved by using the optimized filter. The methodology described in this thesis allows for an improved emitters/filters design procedure for selected applications.

ÖZET

YÜKSEK VERİMLİ GÜÇ ÜRETİM CİHAZLARI İÇİN, IŞININ DALGABOYUNA GÖRE SEÇİCİ DAVRANAN KAPLAMALARIN TASARIMI

Bu tez, ışının dalgaboyuna göre seçici davranan ışıyan ve filtre eden yapıların, thermophotovoltaic (TPV) gibi optik ve ısı uygulamalarındaki tasarımını ve optimize edilmesi hedeflemektedir. Bu cihazlarda dalgaboyuna göre seçici ışıyan ve filtre eden yapılar kullanmak, optiumum bir sisteme ulaşmak için oldukça önemli bir adımdır. Sunulan Si/SiO_2 bazlı filtre konsepti, proses için gerekli enerjiyi minimize etmek amacıyla, çevrilemeyen aralığın büyük bölümünü ışıyıcıya geri yansıtır aynı zamanda da kesme dalgaboyu değiştirilebildiğinden değişik sıcaklıklardaki farklı tipten hücre ve ışıyıcılara adapte edilebilir. Bu çalışma ana olarak InGaSb bazlı TPV hücrelere odaklansa da, Si, GaSb, and $Ga_{0.78}In_{0.22}As_{0.19}Sb_{0.81}$ bazlı hücreler de incelenmiştir. Simülasyonlar TPV cihazlarda bu tip filtreler kullanılarak genel system ve cihaz verimliliğinde kaydadeğer gelişme olduğunu göstermiştir. Ek olarak, grafen bazlı dalga boyuna göre seçici yapılar, dar dalgaboyu aralığında ışık emilimi ve geçişi elde edebilmek için teorik açıdan incelenmiştir. Spektral emilim ve geçişi tanımlayabilmek için iki konsept tanımlanmış ve sonuçta yüzey yapıları ve grafen katmanları ile bu 2 boyutlu, çok katmanlı yapıların dar bant aralığında emilim ve geçiş yapabilmekte olduğu gösterilmiştir. Işınım yapan yapılar için grafen katmanının etkisi güç yitimi profilleri kullanılarak tanımlanmıştır. Önerilen filtre yapısı daha sonra TPV sistemi için optimize edilmiş ve genel TPV verimliliğinin optimize edilmiş filtreler kullanarak geliştirilebildiği görülmüştür. Bu tezde açıklanılan metodoloji, seçilmiş uygulamalar için gelişmiş bir ışıma ve filtrasyon tasarım prosedürü sağlamaktadır.

TABLE OF CONTENTS

ACKNOWLEDGEMENTS . . . iii
ABSTRACT . . . iv
ÖZET . . . v
LIST OF FIGURES . . . viii
LIST OF TABLES . . . xiii
LIST OF SYMBOLS . . . xiv
LIST OF ACRONYMS/ABBREVIATIONS . . . xvii
1. INTRODUCTION . . . 1
1.1. Solar powered energy systems - Photovoltaic systems . . . 2
1.2. Heat-to-power units - Thermophotovoltaic systems . . . 7
2. LITERATURE SURVEY AND RESEARCH OBJECTIVES . . . 11
2.1. Literature survey . . . 11
2.2. Research objective . . . 18
2.3. Organization of the dissertation . . . 18
3. GOVERNING EQUATIONS . . . 19
3.1. Maxwell equations . . . 19
3.2. Rigorous coupled wave analysis (RCWA) . . . 21
3.3. RCWA Formulation . . . 22
3.4. Verification studies . . . 26
4. DESCRIPTION OF A TPV SYSTEM . . . 29
4.1. 1D Multilayer Si/SiO_2 Photonic Crystals . . . 30
4.2. Thermal modeling of a thermophotovoltaic system . . . 30
4.3. Detailed balance principle and fundamental losses in photovoltaic devices 32
5. OPTIMIZATION OF SPECTRALLY SELECTIVE Si/SiO_2 BASED FILTERS FOR THERMOPHOTOVOLTAIC DEVICES . . . 34
5.1. Objectives . . . 34
5.2. Methodology . . . 35
5.3. Results and discussion for Si/SiO_2 based multilayered structures . . . 35
5.3.1. Filter design . . . 35

5.3.2. Performance evaluation of the filters 41
5.3.3. Simulation of the suggested filter design in TPV devices with other cell materials 43
6. ENHANCEMENT OF SPECTRAL ABSORPTION AND TRANSMISSION OF GRAPHENE BASED NANO-STRUCTURES IN NARROW-BANDS . . 50
6.1. Objectives 50
6.2. Graphene-layer systems 50
6.3. Verification study of the application of the Drude model and Kubo formula 53
6.4. Results and discussions for Gr-based structures 55
6.4.1. Spectrally selective emitter 55
6.4.2. Spectrally selective filter 60
7. CONCLUSIONS AND RECOMMENDATIONS FOR FUTURE WORKS . . 67
7.1. Conclusions 67
7.2. Future works 70
REFERENCES 72

LIST OF FIGURES

Figure 1.1. Solar power distribution on earth [1]. 3

Figure 1.2. Solar radiation power spectrum [2]. 3

Figure 1.3. Planck's blackbody distribution at different temperatures [3]. . . . 4

Figure 1.4. A p-n junction [4]. 5

Figure 1.5. (a) A TPV device schematics with spectrally selective filter, (b) blackbody spectral emissive power, (c) transmitted (orange area) and reflected (green area) wavelengths of the blackbody emissive power by the spectrally selective filter with cut-off wavelength of λ. 8

Figure 1.6. (a) A TPV device schematics with spectrally selective emitter, (b) emitted power by spectrally selective emitter with cut-off wavelength of λ. 9

Figure 3.1. List of the methods and their specifications to solve Maxwell equations. 22

Figure 3.2. (a)The Multilayered Si/SiO_2 structure considered by Mao and Ye [6], with $d_{Si} = 0.17\mu m$, $d_{SiO_2} = 0.39\mu m$ (b) Transmittance with respect to the wavelength for RCWA code used in the present study and The results of Mao and Ye. 27

Figure 3.3. (a) The W rectangular grating suggested by Wan [14], (b) Absorptance with respect to the wavelength for RCWA code used in the present study and The results of Wan ($a_0 = 1\mu m$, $d = 0.5\mu m$, $h = 0.5\mu m$, and $b = 0.3\mu m$). 28

Figure 4.1. Schematic of the TPV system considered. 29

Figure 5.1. (a) 10 layered structure with five Si/SiO_2 units (design 1), (b) transmittance and absorptance spectrum of design 1 structure. 36

Figure 5.2. Refractive index of Si [59]. 37

Figure 5.3. Refractive index of SiO_2 [59]. 37

Figure 5.4. (a) Transmittance contour plot of the structure with five Si/SiO_2 units (design 1) when λ_1 is changing, (b) transmittance with $\lambda_1 = 3.6\mu m$, (c) transmittance with $\lambda_1 = 2.21\mu m$. 38

Figure 5.5. (a) 20 layered structure with two sets of five Si/SiO_2 units (Design 2), (b)Transmittance and absorptance spectrum of Design 2. . . . 40

Figure 5.6. Output electrical power (P_{out}) with respect to the emitter temperature (T_e) for different filter cases. 42

Figure 5.7. Input power to the system (q_{th}) with respect to the emitter temperature (T_e) for different filter cases. 43

Figure 5.8. Overall efficiency (η) with respect to the emitter temperature (T_e) for different filter cases. 44

Figure 5.9. The cell temperature (T_s) with respect to the emitter temperature (T_e) for different filter cases. 45

Figure 5.10. Fundamental losses and maximum electrical power output with respect to the cell temperature in the InGaSb cell for $T_e = 1800K$, normalized with incident radiation. 45

Figure 5.11. Fundamental losses and maximum electrical power output of the systems with different types of filters for $T_e = 1800K$, normalized with q_{th}. 46

Figure 5.12. Overall efficiency (η) (see Equation 4.1) with respect to the emitter temperature (T_e) with different filter cases for Si. 47

Figure 5.13. Overall efficiency (η) (see Equation 4.1) with respect to the emitter temperature (T_e) with different filter cases for GaSb. 48

Figure 5.14. Overall efficiency (η) (see Equation 4.1) with respect to the emitter temperature (T_e) with different filter cases for $Ga_{0.78}In_{0.22}As_{0.19}Sb_{0.81}$. 48

Figure 6.1. Schematic of the Ag and Gr structures considered by Zhao *et al.* [42] and absorptance spectrum. 51

Figure 6.2. Schematic of the structures considered. Design 3(a), and Design 4(b). 52

Figure 6.3. The Ag grating structure with $h = 0.2\mu m$, $b = 0.03\mu m$, and $\Lambda = 0.4\mu m$ covered with a Gr layer suggested by Zhao *et al.* [42] , (b) Absorptance with respect to the wavelength for RCWA code of the present paper and Zhao *et al.*'s paper. 54

Figure 6.4. Absorptance contour plot showing the effect of Si film thickness (t_{Si}) with respect to the wavelength in Design 3 structure. 56

Figure 6.5. Absorptance spectrum of the structure shown in Design 3 (Figure 6.2(a)) and the structure introduced by Zhao *et al.* [42]. 57

Figure 6.6. The effect of the Gr layer on absorptance of the Design 3 structure shown in Figure 6.2(a). 57

Figure 6.7. The absorptance spectrum of each separate layer of the Design 3 structure shown in Figure 6.2(a). 58

Figure 6.8. Power dissipation profile of the Design 3 structure at the wavelength of $2.58\mu m$ for without Gr (a) and with Gr (b) cases. The section indicated by the rectangular dashed line in (b) is magnified in (c). 59

Figure 6.9. Power dissipation profile of the Design 3 structure at the wavelength of $1.31\mu m$ for without Gr (a) and with Gr (b) cases. The section indicated by the rectangular dashed line in (b) is magnified in (c). 60

Figure 6.10. Absorptance spectrum of the Design 4 structure shown in Figure 6.2(b) with $h = 0.16\mu m$, $b = 0.007\mu m$, $\Lambda = 0.5\mu m$. 61

Figure 6.11. The effect of the Gr layer on absorptance of the Design 4 structure shown in Figure 6.2(b) with $h = 0.16\mu m$, $b = 0.007\mu m$, $\Lambda = 0.5\mu m$. 61

Figure 6.12. Power dissipation profile of the Design 4 structure at the peak absorptance wavelength ($1.78\mu m$) for without Gr (a) and with Gr (b) cases. The sections indicated by the rectangular dashed line in (b) are magnified in (c). 62

Figure 6.13. Transmittance spectrum of the Design 4 structure shown in Figure 6.2(b) with $h = 0.29\mu m$, $b = 0.1\mu m$, $\Lambda = 0.5\mu m$ 63

Figure 6.14. Considered structure in Figure 6.2(b) (Design 5) with Si/SiO_2 multilayered structure. 64

Figure 6.15. Transmittance spectrum of the Design 5 structure shown in Figure 6.14 for changing t_{gap}. 65

Figure 6.16. Transmittance spectrum comparison of the Design 4 structure shown in Figure 6.2(b) (blue dashed line) with the Design 5 structure shown in Figure 6.14 (green solid line). 65

Figure 6.17. Overall efficiency of a GaSb based TPV cell with, no filter, ideal filter, the Design 2 filter, Design 4 filter, and Design 5 filter. 66

Figure 7.1. Considered cases in performance comparison for Si/SiO_2-based filters. 67

Figure 7.2. Considered cases in performance comparison for Gr-based filters. . 69

LIST OF TABLES

Table 4.1. Fundamental losses in a PV cell [57]. 33

Table 5.1. Varshni equation constants for Si, GaSb, and $Ga_{0.78}In_{0.22}As_{0.19}Sb_{0.81}$. 47

Table 5.2. Optimized layer thicknesses for different cell types. 47

LIST OF SYMBOLS

a_0	Grating pitch
$\vec{B}$	Magnetic flux density
Bi	Biot number
b	Gap distance between gratings
c	Light speed in the vacuum
$\vec{D}$	Electric flux density
d_{Si}	Si layer thickness
d_{SiO_2}	SiO_2 layer thickness
d_{tot}	Total thickness of the filter
$\vec{E}$	Electric field intensity
$E_{b,c}$	Black body emissive power of the cell
$E_{b,e}$	Black body emissive power of the emitter
$E_{b,f}$	Black body emissive power of the filter
$E_g(0)$	Band-gap energy at absolute zero
e	Electro charge
G	Reciprocal lattice vector
G_e	Irradiation to the emitter
G_s	Irradiation to the filter/cell structure
$\vec{H}$	Magnetic field intensity
h	Planck's constant
h	Grating height
h_c	Convective heat transfer coefficient
$\vec{J}$	Electric current density
J	Photocurrent generated in the cell
J_e	Radiosity of the emitter
J_s	Radiosity of the filter/cell structure
k	Attenuation coefficient
k_0	Free-space wave number

k_b	Boltzmann's constant
k_f	Effective thermal conductivity
L_a	Above λ_g loss
L_c	Carnot loss
L_e	Emission loss
L_{th}	Thermalization loss
n_{Si}	Refractive index of the Si
n_{SiO_2}	Refractive index of the SiO_2
P_d	Power dissipation
P_{out}	Output electrical power
q_{th}	Heat provided by external source
T	Temperature
T_a	Ambient temperature
T_e	Emitter temperature
T_s	Filter/cell structure temperature
t_{gap}	Gap distance
t_{Si}	Si layer thickness
V	Applied voltage
V_{max}	Voltage across the cell at maximum power point
w	Grating width
α_E	Material specific constant
α_f	Absorptance of the filter
$\alpha_{\lambda f}$	Spectral absorptance of the filter
$\alpha_{\lambda,n}$	Normal spectral absorptivity
β_E	Material specific constant
γ	Scattering rate
Δ	Gr layer thickness
ε	Dielectric constant
ε''	Imaginary part of the dielectric function
$\bar{\varepsilon}$	Permittivity

ε_0	Vacuum permittivity
ε_f	Emittance of the filter
ε_r	Relative permittivity
ε_∞	High frequency constant
η	Overall efficiency
Λ	Grating pitch
λ	Wavelength
λ_0	Central wavelength of the band-gap
λ_1	Wavelength of the lower edge of the first stop-band
λ_g	Band-gap wavelength
μ	Chemical potential
$\bar{\mu}$	Permeability
μ_0	Vacuum permeability
μ_r	Relative permeability
ρ_v	Electric charge density
σ	Electrical conductance
$\vec{\sigma}$	Conductivity
σ_{Drude}	Drude part of the electrical conductance
σ_{Inter}	Interband part of the electrical conductance
τ	Relaxation time
$\tau_{\lambda f}$	Spectral transmittance of the filter
ϕ_{abs}	Absorbed photon flux
ϕ_{emit}	Emitted photon flux
ω	Angular frequency
ω_p	Plasma frequency
∇	Gradient
$\hbar$	Reduced Planck's constant

LIST OF ACRONYMS/ABBREVIATIONS

1D	One Dimensional
2D	Two Dimensional
CEM	Computational Electro Magnetic
CHP	Combined Heat and Power
DDA	Discrete Dipole Approximation
EHP	Electron-hole pairs
EM	Electromagnetic
FDTD	Finite Difference Time Domain
FEM	Finite Element Method
GA	Genetic Algorithm
IR	Infrared
PV	Photovoltaic
TE	Transverse Electric
TM	Transverse Magnetic
TPV	Thermophotovoltaic

1. INTRODUCTION

Energy has been playing a significant role on human progress especially in the last few centuries. Before the industrial revolution, which started around 1760's, humans were using carbon based fuels such as wood, straw etc. for warming houses or other thermal processes such as for cooking or ironworks. For transportation, they relied on animal power on land and wind on oceans. Most of the science historians believe that learning how to harness and control energy was one of the essential causes of the industrial revolution. Discovery of fossil fuels commenced by coal can be considered as a revolutionary phenomenon that changed the course of the history, and coal was the main energy source of the first steam engines relying on power cycles. Although many other ways of generating useful work have been developed in the following centuries, it is still one of the base sources of the industry due to its abundance and reduced price in comparison to the other energy sources. The importance of fossil fuels increased further with the expansion of internal combustion engines and by exploration of other types of fossil fuels such as oil and natural gas.

Technology enabled low cost fossil fuel extraction and refinement to meet the growing demand on energy that led to an economy heavily relying on fossil fuels. However, concerns in regards to climate change and environmental safety also increased in the last decades as use of fossil fuels have led to an increase in the atmospheric concentration of carbon dioxide, which is a primary greenhouse gas, and pollutants such as carbon monoxide, sulphur dioxide, and nitrogen oxides. There are different approaches to overcome these problems, such as using alternative energy sources, recycling of waste heat and enhancement in the energy conversion efficiency.

In addition to lighting the earth, ancient humans realized the potentials of the solar energy. In 7th century B.C. they started to use solar energy to light fires using magnifying transparent materials. Similar concept is then developed to power the ovens in 1700s. Basically, new page is turned in renewable energy course when in 1876, William Grylls Adams and his student discovered that electricity can be produced when

selenium is exposed to light. In 1953 Calvin Fuller, Gerald Pearson, and Daryl Chapin discovered that Silicon is much more efficient than selenium to generate electricity. Ever since then, Silicon become an unavoidable part of the solar power generation as todays solar power plants are based on this material. Nowadays, solar power is turned to a popular way of generating electricity because of its tremendous specifications such as being pollution free, freely available in almost everywhere, having low maintenance costs, etc.

As mentioned earlier, one ways to reduce the large effects of fossil fuel use is to increase the use of energy produced from renewable sources. Solar energy can be considered as one of the most important sources in this category, since it is available at most of the populated places on the earth. Figure 1.1 shows the incident solar irradiation distribution over the earth and it illustrates that almost all of the populated regions are shined by immense amount of solar energy. However, one of the most important drawbacks of the solar energy is its relatively high cost per produced power with respect to the fossil fuels due to high cost and limited efficiency of the solar power plants. Nevertheless, it seems that it is still an important competitor of the fossil fuels due to the drastic effects of the fossil fuels on environment. Last decades witnessed a major development on solar harvesting technology that lead to more efficient systems, which in turn decreases the energy costs.

1.1. Solar powered energy systems - Photovoltaic systems

As discussed above, due to its abundance on the earth, utilization of solar energy is growing with a fast pace. In order to have deeper insight into the solar powered energy generation systems, it is necessary to understand the solar radiation. Figure 1.2 shows the solar power spectrum reaching the earth surface. Basically, sun can be approximated as a black body source at about $5800K$ as shown in the figure [3]. Due to the different ingredients available in the atmosphere, some portion of the solar power is absorbed or reflected back to the outer space as illustrated in the figure. As can be seen, the majority of incident solar power is in visible wavelength range (0.4-$0.7\mu m$). Since the molecules in the atmosphere are almost transparent at visible

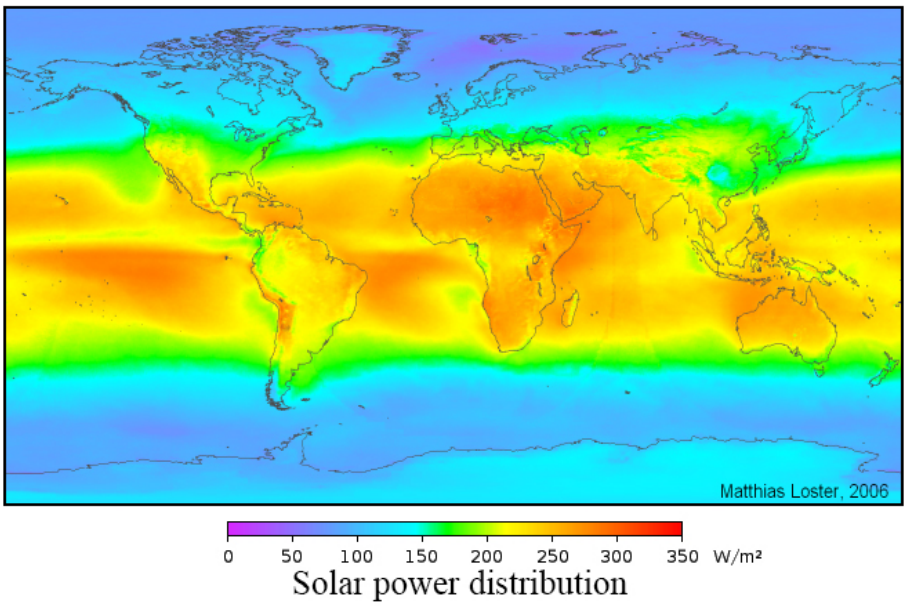


Figure 1.1. Solar power distribution on earth [1].

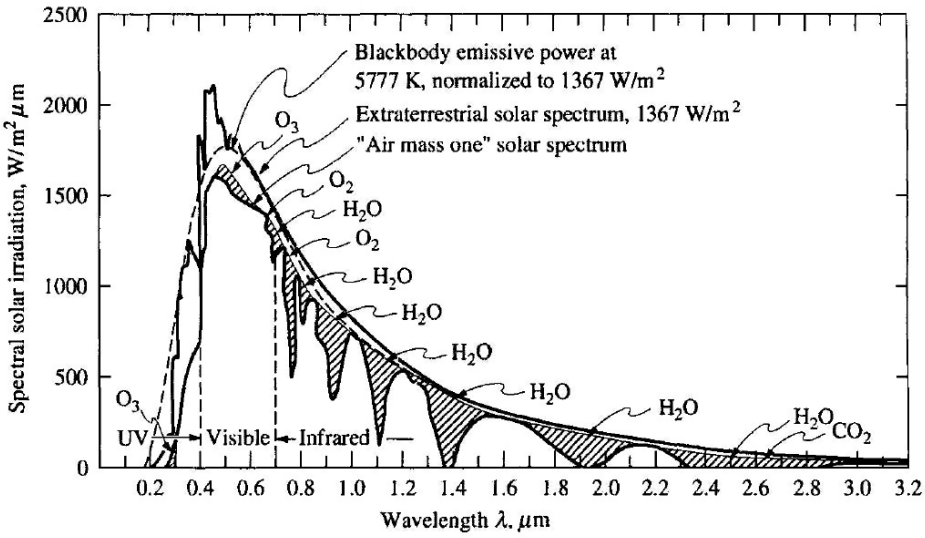


Figure 1.2. Solar radiation power spectrum [2].

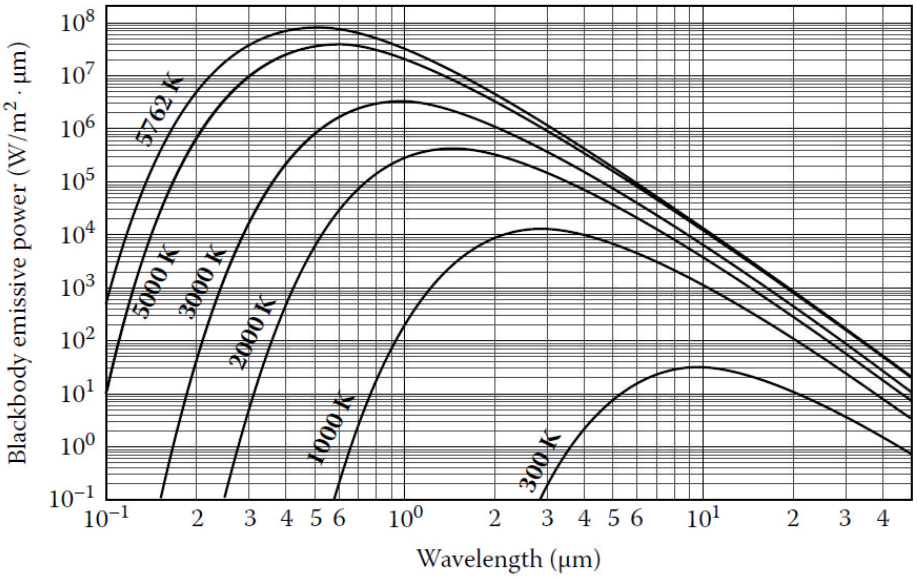


Figure 1.3. Planck's blackbody distribution at different temperatures [3].

range, the radiation passes through it and reaches to the earth surface and heats the surface. However, since the heated surface is in the reduced temperature $(300-320K)$, therefore it emits majorly on long wavelengths as shown in the Figure 1.3. Some gases in the atmosphere such as CO_2, called greenhouse gases, are not transparent for such long wavelengths. Consequently, the solar radiation is banned in the atmosphere which leads the temperature of the atmosphere to be increased. This phenomenon is called greenhouse effect that leads to global warming. By burning fossil fuels to drive the industry, human release more CO_2 to the atmosphere which intensify the greenhouse effect. Focusing on renewable energies can be a critical solution to overcome global warming. Harvesting the solar energy plays an important role on diminishing this phenomenon.

Generation of electricity by solar energy can be categorized by two major approaches:

- Solar thermal systems
- Photovoltaic systems

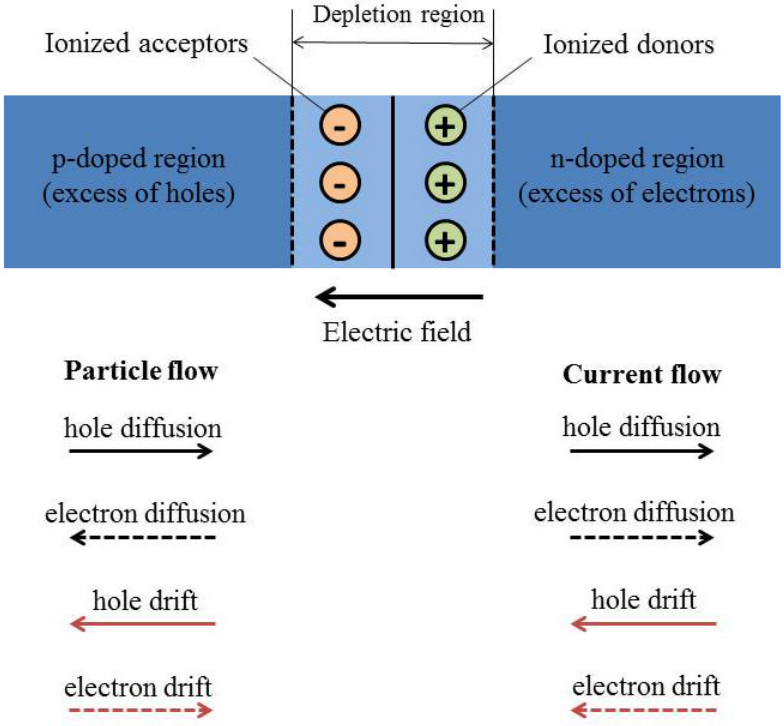


Figure 1.4. A p-n junction [4].

Solar thermal systems use the solar energy in order to heat a working fluid of a thermodynamic system. The heated fluid is then drives a heat engine where the useful work is produced as electricity.

Solar photovoltaic (PV) devices are one of the promising devices to generate electricity from the energy emitted from the sun. The photovoltaic effect was first introduced by Becquerel in 1839. However, the first solar cell was produced by Fritts in 1883 by coating the selenium with an extremely thin layer of gold to form the junctions, although the produced device was only around 1% efficient. Since then, Several researchers developed different types of structures with different materials to improve the converting efficiency of the devices.

The PV devices directly convert the radiative energy to electricity using semi-conductor materials under the concept of photovoltaic effect. A PV cell composed of two semi-conductor layers as shown in Figure 1.4. One is positively doped (p-doped) and the other negatively doped (n-doped). P-doped materials can be made by group

III impurities of periodic table which have 7 valence electrons or one hole, which are ready to accept an electron. N-doped materials are made of group V impurities of periodic table having 9 valence electrons, meaning they have one extra electron ready to donate to be stable. When the two opposite doped layers are brought into contact, the holes flow from the p-doped region, where they are in excess, to the n-doped region, where their concentration is low. This is also the case for the electrons flowing from n-doped region (high in electron concentration) to p-doped region (low in electron concentration). This process continues until equilibrium is reached. A new region is created near the junction spanning narrow part of the both p-doped and n-doped layers called depletion region due to the flow of electrons. Ionized acceptors (p-region) are located at the top and ionized donors (n-region) are located at bottom of the region. This charge gradient generates an electric field opposing the diffusion direction of electrons and holes. At equilibrium, current of electrons and holes (called diffusion current) exactly cancels the current of ionized particles (called drift current). However, in the presence of radiation incidence, electron-hole pairs (EHPs) are created within depletion region if the energy of incoming photons is equal to or above the band-gap of the semiconductor. The band-gap energy is the minimum amount of energy required to excite and free an electron in the semiconductor leading to electrical conduction. The corresponding wavelength of the photon with the band-gap energy is called the band-gap wavelength. The created EHPs are split by the electric field at the junction causing aggregation of electrons in the n-doped side and vice-versa for holes. If the positive and negative regions of depletion region are connected to an electrical load, the drift of EHPs can create usable electric potential.

The common PV materials are mono- and poly-crystalline silicon, amorphous silicon, InGaSb, GaSb, $Ga_{0.78}In_{0.22}As_{0.19}Sb_{0.81}$. Structuring the device geometrically and using proper materials can enhance the solar energy absorption significantly leading to increase in PV overall efficiency.

1.2. Heat-to-power units - Thermophotovoltaic systems

As discussed earlier, another approach to reduce the use of fossil fuels and their destructive effects on environment is enhancing the efficiency of the systems by recycling the waste energy. One of the important devices in this category is the thermophotovoltaic (TPV) systems, which converts the wasted heat to electrical power.

The first TPV device was built by Kolm at the Massachussets Institute of Technology (MIT) [4]. He used silicon as the PV cell and lantern as a radiator. Although his device was low efficient, it is considered as a breakthrough to directly convert thermal energy to electricity in the literature.

The TPV devices function based on same principles with the PV devices. However, instead of the solar energy, which is predominantly in the visible spectrum, TPV devices rely on radiation from thermal sources to generate electricity. As the Figure 1.3 shows, thermal sources have reduced temperatures with respect to the sun, and emit at longer wavelengths. Based on the photovoltaic effect, a PV cell can convert the radiation with wavelength lower than the band-gap wavelength of the cell to electricity. However, the radiation with higher wavelengths, heat the cell, which reduce its conversion efficiency. Therefore, the incoming radiation from a heat source should be ideally less than band-gap wavelength of the cell to maximize the conversion efficiency. To overcome this problem, two different types of TPV systems have been considered, as shown in Figures 1.5 and 1.6. The first type consists of a spectrally selective filter and a PV cell in addition to the heat source (Figure 1.5(a)). The heat source is a broad band emitter that can be approximated as a blackbody (blue area in the diagram of Figure 1.5(b)) and the filter only transmits the radiation with wavelengths lower than the band-gap wavelength of the cell (orange area in the diagram of Figure 1.5(c)) and reflects the rest of the radiation (green area in the diagram of Figure 1.5(c)) back to the heat source. As the PV cell can convert all of the orange area to the electricity; therefore, the maximum efficiency of the TPV device will be achieved.

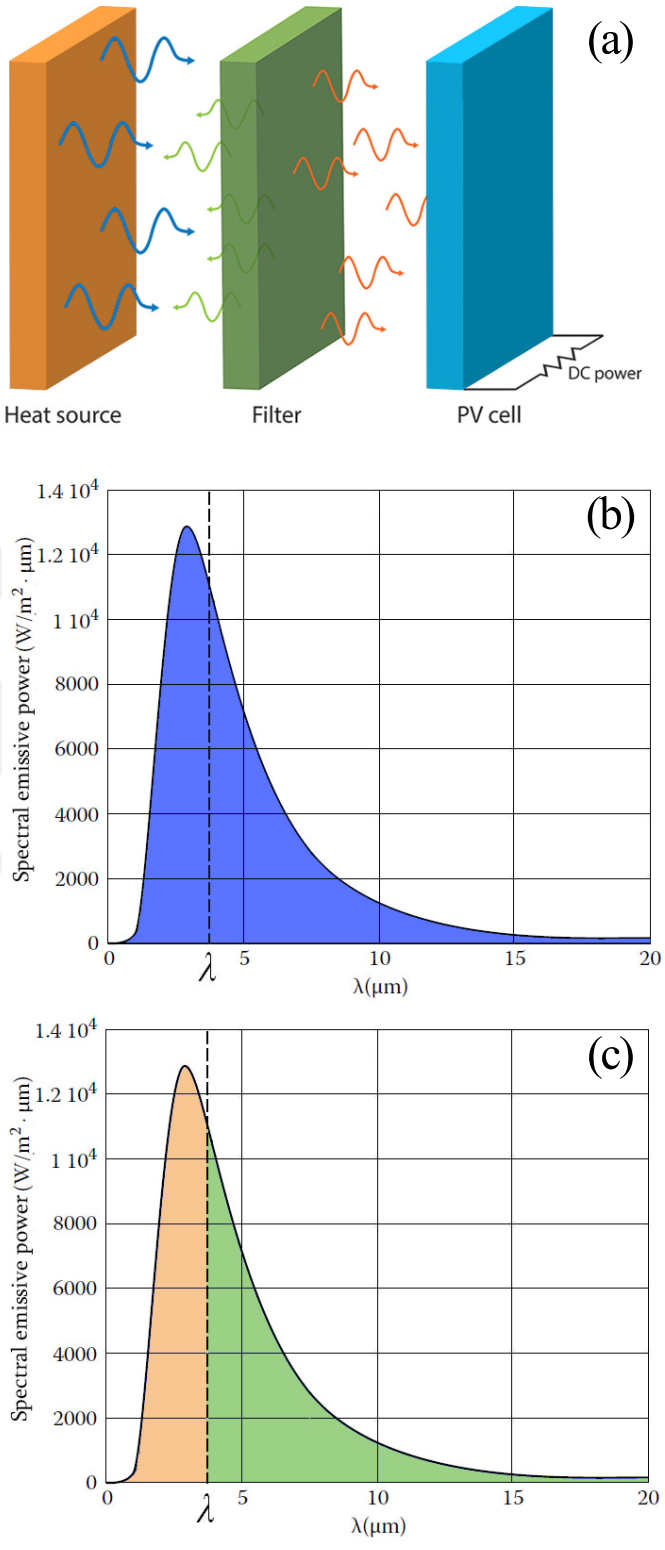


Figure 1.5. (a) A TPV device schematics with spectrally selective filter, (b) blackbody spectral emissive power, (c) transmitted (orange area) and reflected (green area) wavelengths of the blackbody emissive power by the spectrally selective filter with cut-off wavelength of λ.

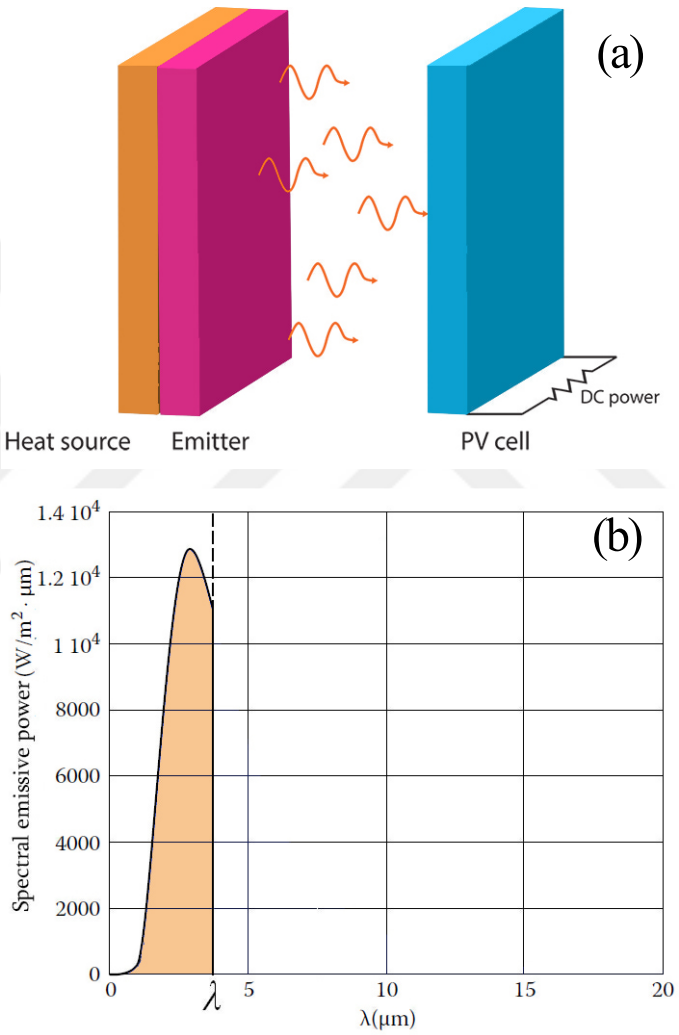


Figure 1.6. (a) A TPV device schematics with spectrally selective emitter, (b) emitted power by spectrally selective emitter with cut-off wavelength of λ.

Second type of the TPV devices consist of a spectrally selective emitter attached to the heat source rather than a filter as shown in Figure 1.6(a). As the diagram also indicates, the spectrally selective emitter ideally emits only at the wavelengths lower than the band-gap wavelength of the PV cell (orange area in the diagram of Figure 1.6(b)) and since the PV cell is not exposed to the undesired wavelength at higher wavelengths, it will perform with its maximum efficiency. Following advantages can be mentioned for TPV systems:

- Low maintenance due to the absence of any moving part
- High power density
- Pollution free
- Lightweight
- Quite, since no moving part is involved
- Can be applied for any high temperature source.

Although the use of TPV devices dates back to 1960 [4], the nano-technology plays a substantial role on developing TPV power systems during last decade. The most challenging problem for TPV systems is designing a proper spectrally selective filter/emitter according to the band-gap wavelength of the PV cell due to its significant effect on the TPV system overall efficiency. This study aims at designing nano-structured spectrally selective filters/emitters for TPV devices via optimization considering the cell material. Exploring the literature published in recent years demonstrates how designing of micro- nano-structures is momentous in TPV devices. In the next chapter a literature survey is presented in regards to the filter/emitter design.

2. LITERATURE SURVEY AND RESEARCH OBJECTIVES

2.1. Literature survey

As mentioned earlier, the objective of the present study is to design nano-structured spectrally selective filters/emitters for TPV devices. Several researchers have explored the fundamentals and applications of spectrally selective photonic crystals. In the available literature, nano-scale engineering methods are applied to develop advanced materials in order to enhance the efficiency of the TPV devices.

One dimensional structures are frequently considered by some researchers due to their simplicity in manufacturing. They may be categorized as vertically mounted multilayered structures [5–12] and laterally formed structures [13–16] or combination of both [17–19].

One of the major applications of the 1D structures are designing spectrally selective filters to manipulate the transmittance. O'Sullivan *et al.* [5] numerically and experimentally studied a filter with multiple Si/SiO_2 and Si/SiON layers. While a wide stop-band wavelength range between $1.8 - 3.3\mu m$ is captured by the Si/SiO_2 filter, at higher wavelengths ($> 3.5\mu m$) this configuration leads to undesired transmittance. The designed filters are applied for GaSb and InGaAsSb cells and showed that Si/SiO_2 filter has improved spectral efficiency. Mao *et al.* [6] modified their Si/SiO_2 structure by changing the thickness of the layers and were able to remove the fluctuations of reflectance around $1.45 - 1.75\mu m$ that slightly enhanced the power density and spectral efficiency of the TPV cell. GuangPing *et al.* [7] used a structure composed of four Si/SiO_2 sets with different thicknesses of Si and SiO_2 layers. While the designed filter has satisfactory transmission performance between the $0.9 - 1.8\mu m$, the effects at higher wavelengths ($> 3.3\mu m$) are not considered. Mostafa *et al.* [8] investigated another 1D structure composed of Ag/SiO_2 layers designed for a GaSb based TPV sys-

tem. They achieved about 78% of transmittance in above band-gap wavelength range that leads to a spectral efficiency of 66%. Wang *et al.* [9] examined three different multilayered selective filters composed of periodic layers of ZnS/Na_3AlF_6, TiO_2/SiO_2, and Nb_2O_3/SiO_2 for a Si TPV system. Acceptable stop-band range is achieved in the wavelength range of $1.1 - 2.75\mu m$ by applying ZnS/Na_3AlF_6 and TiO_2/SiO_2 multilayered coatings; whereas, wider transmittance was observed for $0.4 - 1.1\mu m$ band with some unwanted transmitted radiation at the higher wavelengths for the case of Nb_2O_3/SiO_2 coating.

Selective emitters can be built from one-dimensional structures. Vertically mounted multilayered structures are used as emitter rather than filter in some studies [10–12]. Sakr *et al.* [10] suggested a 1D structure composed of Sm-doped glass sandwiched between two dielectric multilayers, as a selective emitter for a GaSb cell and achieved an overall efficiency of 38.5% for an emitter temperature of $1573K$. They also introduced an emitter comprised of W rectangular gratings coated by SiO_2 and TiO_2 leading to 38% TPV efficiency for the same emitter temperature with GaSb cell. Kocer *et al.* [11] proposed a multilayered structure composed of Cr, PMMA (Poly methylmethacrylate), Au over a Sapphire substrate. This structure showed almost perfect absorptance at the wavelength of $1.2\mu m$, while it has zero absorptance at $1.8\mu m$. Rare earth materials have also been considered due to their potential to fulfill the spectrally selective emitter demands. Foley *et al.* [12] applied rare earth materials based selective coatings, comparing several types of emitters composed of Ag, W, Si_3N_4, YSZ, and Ta layers and claimed that an emitter with YSZ/Ag/YSZ/W layers is favorable for GaSb and InGaAsSb cells, considering emitter temperatures of $1000K$ and $1750K$, for a solar concentration ratio of 1000 and 2500, respectively.

Several researchers focused on functionalities of laterally formed 1D structures. Sai *et al.* [13] have performed a parametric study on the 1D W rectangular grating showing that high absorption can be achieved due to surface plasmon polaritons and they showed that the absorption peak, can be shifted to other wavelengths by changing the structure. Wan *et al.* [14] studied a similar W rectangular grating as an emitter and showed that by changing the groove depth, emittance at particular wavelengths can be

enhanced. Zhao and Zhang [15] studied Ag and doped Si based rectangular deep gratings and obtained narrow-band absorptance peak at near-IR wavelength range. They showed that by changing the geometric parameters of the structures, absorptance peak can be tuned between near-IR to microwave range. Nguyen-Huu *et al.* [16] suggested a structure with pyramid gratings made of W and Ni. They achieved good absorptance between $0.6 - 1.72\mu m$ and low absorptance (around 10%) for the wavelengths greater than $2.5\mu m$. Wang and his research group proposed VO_2 based multilayered structures with VO_2 and Au strips instead of using bare grating structures in two separate studies [17], [18]. In [17], the structure is composed of 1D VO_2 periodic gratings on MgF_2 and VO_2 layers, where they showed that, an absorption peak occurred at $10.9\mu m$, when VO_2 is metal. However, at temperatures lower than $341K$, VO_2 turns to dielectric phase, and the absorption peak shifts to the $15.1\mu m$. In another study [18], Wang *et al.* used Au periodic grating on stacked VO_2 and Au layers. At the temperatures lower than $341K$, the absorption peak exists at $5\mu m$. As the temperature of the structure increases above $341K$, the absorption peak disappears. They claimed that the peak point also can be tuned by changing the geometric parameters of the gratings. In a parallel study, Song *et al.* [19] designed an emitter with SiO_2 strips sandwiched between W strips and W substrate, optimizing the structure to capture the desired spectral behavior for a GaSb cell. They showed that the emittance of the structure reaches approximately 100% between $0.9 - 1.8\mu m$, whereas it drops slightly at higher wavelengths.

Use of 2D structures is also investigated in the literature. Some studies considered bare 2D structures such as those by Sai and his research group [20–22]. Rectangular and circular microholes on W plates are investigated in [20], and [20]. The samples were manufactured by fast atom beam etching using two different lithography techniques. While their experimental and numerical results match, they also carried out a parametric study in order to identify optimum shape. Heating tests conducted under vacuum condition revealed high thermal stability of W and the designed structures are suitable for both PV and TPV devices. In another experimental study [22], they presented the enhancement in efficiency of the InGaAs TPV cell using a filter with W gratings and it was shown that the spectrally selective properties of the filter is slightly suppressed

at elevated temperatures. Similar structure is considered by Heinzel *et al.* [23]. They investigated the performance of a W layer with cylindrical gratings experimentally and numerically using rigorous coupled wave approach (RCWA) and reported that the investigated system was a good selective emitter with strong directional dependence. Some studies showed that using metallic plates with cylindrical holes similar to the studies presented above filled with dielectrics can improve the spectral behavior. Yeng *et al.* [24] presented such structure composed of a Ta plate with cylindrical holes filled with HfO_2, which is a dielectric material. The suggested structure is insensitive to the incidence angle and polarization. The emittance reaches 86% for the wavelengths below the cut-off wavelength and 12% for the rest of the spectrum by optimizing the structure according to the desired cut-off wavelength. In another similar study wide-angle absorption is obtained by Chou *et al.* [25]. The structure is composed of a metal layer with cylindrical holes filled with a dielectric material, and good absorption is achieved between $0.5 - 2.3\mu m$, which is almost independent of the angle of incidence. Fang *et al.* [26], [27] considered dielectric structures, instead of metallic ones. They studied four crystalline Si structures; circular nano-wire array, circular nano-hole arrays, square nano-wire arrays, and square nano-hole arrays in [26]. They showed that square nano-wire arrays and circular nano-hole arrays with lattice constant of 600nm have better spectrally selective absorptance. Moreover, they also explored amorphous Si plate with disordered nano-hole patterns; non-uniform radius, random position, and amorphous pattern [27]. They showed that relatively smooth absorption over entire incident spectrum can be achieved by using disordered pattern instead of ordered pattern.

More complex structures composed of coated 2D gratings with different shapes are suggested by different studies to satisfy a diverse range of spectral behavior. Sai and his research group also considered a Si plate with reverse pyramid cavities coated with Pt thin film using Si anisotropic etching and laser ablation techniques in [28]. The experimental data are matched by numerical model using RCWA. Significant enhancement in absorptance is reported for cavity periods of $2\mu m$ and $1.5\mu m$, at $890K$, with respect to flat Si. Zhao *et al.* [29] introduced an emitter based on a W substrate coated with SiO_2 layer with periodic W cubes placed above that enhances the emittance for

wavelengths shorter than $2\mu m$, which is proper for $In_{0.2}Ga_{0.8}Sb$ cell. Another similar study is carried out by Wang *et al.* [9]. However, instead of using single-sized cubes in each periodicity, they used double-sized W cubes.High absorptance in the visible and near-IR spectrum, and low emittance in the mid-IR range for normal incidence is observed using this structure. Wang and his research group also proposed two different structures in separate papers. A structure made of periodic nano-structured Ti gratings furnished on a MgF_2 layer over W substrate is investigated in [30] and an absorptance higher than 90% within the solar spectrum and emittance of about 20% in the mid-IR range is observed. Moreover, the structure is insensitive to the angle of incidence and polarization within solar spectrum. They also proposed a metamaterial composed of a 2D Al concave grating spaced from an Al substrate by a SiO_2 film [30]. A narrow-band absorptance is observed in the visible and near-IR spectrum. Yang *et al.* [31], applied an emitter with Ge cubes on the Ta substrate achieving high absorptivity at wavelengths shorter than $1.2\mu m$ that is proper for solar-PV systems. Bonakdar *et al.* [32] studied a structure with a Ag meta-surface separated by a SiO_2 layer from an Au layer. The numerical and experimental investigation demonstrated nearly perfect, narrow-band absorption.

Han and Lee [33] considered a 2D multilayered complex grating composed of Au rectangular shapes on SiO_2 spacer and another Au layer as a substrate, where they reported a broadband absorption for normal incident wave. In another study [34], Lee and his group used Ni instead of Au for the complex grating and substrate, and optimized the structure to enhance the absorptance over a wide wavelength range. The absorptance spectrum of the optimized structure is also nearly independent of the incident angle. Ogawa *et al.* [35] considered a mushroom shaped periodic structure comprised of a square micro-patch made of Al connected to the Al plate by the Si posts as a selective infrared absorber. While relatively narrow absorption peak is observed in the near-IR range, they showed that by changing the geometric parameters of the structure, the resonance point can be shifted along the wide wavelength range. Stelmakh *et al.* [36] studied a Ta based photonic crystal with square array of cylindrical holes. Good spectral behavior is reported with a tunable cut-off wavelength. Butun and Aydin [37], and Woolf *et al.* [38] investigated cross-shaped gratings. Butun and

Aydin [37] presented a cross-trapezoid shaped Ag layer over the SiO_2 and another Ag layer. The results showed a good absorptance over wide wavelength range covering the entire visible spectrum. They claimed that by changing the geometric parameters, the spectral absorptance can be changed. Woolf *et al.* [38] investigated an emitter for high temperature applications considering cross-shaped periodic gratings made of Pt placed over an Al_2O_3 thin film and a Pt substrate. The structure is optimized to match the cut-off wavelength of InGaAs based TPV cell. They claimed that at $1300K$ emitter temperature, the overall and spectral efficiency of the TPV device can reach 22%, and 43%, respectively.

VO_2 based 2D structures are also considered by Kocer *et al.* [39] and Ye *et al.* [40]. Two thermally tunable structures composed of Au-VO_2 1D periodic grating, and Au-VO_2 cylinders embedded in VO_2 are proposed in [39]. The absorption resonance around $2.5\mu m$ and $2.3\mu m$ is observed for the first and second structures, respectively. It is also shown that by heating the structures above the phase transition temperature of VO_2, the absorption intensity can be significantly reduced. The suggested structure in [40] consists of a VO_2 plate with periodic cylindrical air micro-cavities. It is shown that the cut-off wavelength is increased by increasing the radius of the cavities and the emissivity at wavelengths below the cut-off wavelength were enhanced by increasing the depths of the cavities.

Due to its unique electrical and optical properties, graphene (Gr) can be used for a number of different applications, including modulators, photodetectors, and PV devices. Specifically, its large electrical transport properties, along with extraordinary mechanical properties, flexibility, and stable characteristics separates Gr from other materials. Gr is an allotrope of carbon and considered as a two dimensional material with hexagonal lattice since its thickness is only about $0.3nm$, roughly the thickness of its molecule. From the optical point of view, Gr acts as an absorptive dielectric and the absorptance of a single sheet is about 2.3% and it is almost uniform along visible and near-infrared wavelength range.

Due to its newly discovered optical properties, researchers have shown increased interest on Gr based spectrally selective emitter/filters during the last decade. Liu *et al.* [41] introduced two structures with Ag strips and Ag rectangular blocks both covered with Gr. They achieved transmittance of about 80% in near- and mid-IR wavelength range. While high transmittance is achieved over a relatively wide-band, they showed that the transmittance peak can be tuned by changing the geometric parameters. Instead of strips, Zhao *et al.* [42] considered Ag deep grating covered with a Gr layer. They obtained narrow-band absorptance at near-infrared range. They claimed that such narrow-band absorption occurred due to the excitation of the magnetic polaritons in the deep metal gratings. Lu *et al.* [43] suggested a more complex structure composed of an Ag layer with groove rings covered with a SiO_2 layer and a Gr layer. The entire structure is placed on a SiO_2 substrate. They reached to the absorptance of about 80% over near-infrared wavelength range.

Instead of metals, in some of the studies, Gr is coated over the dielectric structures. Zhan *et al.* [44] studied two dielectric structures with rectangular grating and periodic rectangular cubic structures over a metal substrate. Both structures are covered with a Gr layer. The maximum absorptance that they achieved is about 90% at mid-IR range. They also showed that the suggested structures are almost independent of the angle of incidence up to 60° for TE polarization. Liu *et al.* [45] considered a simple structure, in which the Gr is placed on top of a Si/SiO_2 multilayered structure with a SiO_2 spacer. They were able to achieve absorptance of about 30% at visible spectrum. They examined different angle of incidence and both TM and TE polarization. The maximum absorptance (30%) is seen at 60° angle of incidence for TE polarization. They claimed that, this absorptance occurred due to the strong photon localization on the dielectric layers. Alaee *et al.* [46] achieved an direction-independent perfect absorption using a structure composed of a dielectric layer covered with Gr strips over Au substrate. The absorptance about 100% is captured in far-IR range. Instead of Gr strips, Thongrattanasiri *et al.* [47] used circular periodic Gr layers on top of the dielectric layer. Their results also showed an absorptance near unity at far-IR range.

2.2. Research objective

When emitters/filters that have transparent bands within IR ranges are used with a TPV cell, the cell receives radiation above its band-gap that reduces its efficiency due to heating. Emitters/filters that exhibit successful spectral selectivity are relatively complex and hard to manufacture [19–22, 26, 36]. This study aims at designing nano-structured spectrally selective filters/emitters for TPV devices via optimization considering the cell material. The overall efficiency of the system is then predicted for the designed filter/emitter. Two structure concepts are introduced in the present study. The first one, which composed of 1D Si/SiO_2 multilayers, is applied as a spectrally selective filter for a InGaSb based TPV system. The second concept is based on Gr nano-layer which can be used as a selective emitter or filter.

2.3. Organization of the dissertation

This dissertation contains seven chapters. Chapter 3 presents the governing equations and theoretical background on electromagnetic wave propagation. Then, the numerical formulation of the rigorous coupled wave analysis (RCWA) method is presented. The thermal modeling of the considered system is discussed in chapter 4. In chapter 5 Si/SiO_2 multilayered structures are considered as spectrally selective filters for TPV applications. Chapter 6 covers the optical behaviors of the Gr-based structures introduced in this study and their advantages on TPV applications.Chapter 9 summarizes the main results of this dissertation and some recommendations for future studies are also presented.

3. GOVERNING EQUATIONS

In order to investigate the optical properties of the designed emitters/filters, Maxwell electromagnetic equations should be solved. In the next section, Maxwell equations are presented and then RCWA method is introduced to solve the equations numerically.

3.1. Maxwell equations

Radiative energy propagation can be described by two approaches: quantum mechanics and classical electromagnetic (EM) wave theorem. In the first approach, the energy is assumed to be transferred by quanta of massless particles called photons, where the interaction of the photons with the medium is approximated by statistical mechanics. However, it is not possible to appropriately predict the energy exchange in the micro- or nano-structures, where there exist polarization, coherence, and tunneling effects [3]. Whereas, EM wave theory can overcome the mentioned shortcomings with a tradeoff of relatively complex calculations [3].

The concept of EM wave theory was first developed by James Clerk Maxwell in 1864, which revolutionized the classical physics. His formulation, known as Maxwell equations, explains the propagating of EM waves in a medium, and relates electric and magnetic fields, showing that EM waves propagate with the speed of light, which equals to about $2.997 \times 10^8 m/s$ in the vacuum. From then on, it was proven numerous times that, the EM wave theory can be used widely in many applications from nano to interstellar dimensions [3]. For radiative transfer, it can be used to predict the reflection, transmission, and absorption behavior of any material, considering directional and spectral variations.

The Maxwell equations in the frequency domain can be presented based on four laws discussed prior to Maxwell [48]:

$$\nabla \times \vec{E} = -j\omega\vec{B} \qquad \text{Faraday's law} \tag{3.1}$$

$$\nabla \times H = \vec{J} + j\omega\vec{D} \qquad \text{Ampere's law} \tag{3.2}$$

$$\nabla \cdot \vec{D} = \rho_v \qquad \text{Gauss's law} \tag{3.3}$$

$$\nabla \cdot \vec{B} = 0 \qquad \text{Gauss's law} \tag{3.4}$$

where $\vec{E}$ is the electric field intensity, $\vec{H}$ is the magnetic field intensity, $\vec{D}$ is the electric flux density, $\vec{B}$ is the magnetic flux density, ρ_v is the electric charge density, $\vec{J}$ is the electric current density, and ω is the angular frequency. For linear and isotropic media, the electric displacement and magnetic induction are related to the electric and magnetic fields by the constitutive relations as the following:

$$\vec{D} = \bar{\varepsilon}\vec{E} \tag{3.5}$$

$$\vec{B} = \bar{\mu}\vec{H} \tag{3.6}$$

where, $\bar{\varepsilon}$ is the dielectric permittivity, and $\bar{\mu}$ is the permeability. The following equation relates the current density to the electric field

$$\vec{J} = \bar{\sigma}\vec{E} \tag{3.7}$$

where, $\bar{\sigma}$ is the conductivity. The $\vec{D}$, $\vec{B}$, and $\vec{J}$ can be replaced in the Equations 3.1-3.4 by Equations 3.5-3.7. The resulted Maxwell equations can be represented as:

$$\nabla \times \vec{E} = -j\omega\bar{\mu}\vec{H} \tag{3.8}$$

$$\nabla \times \vec{H} = \bar{\sigma}\vec{E} + j\omega\bar{\varepsilon}\vec{E} \tag{3.9}$$

$$\nabla \cdot \left(\bar{\varepsilon}\vec{E}\right) = \rho_v \tag{3.10}$$

$$\nabla \cdot \left(\bar{\mu}\vec{H}\right) = 0 \tag{3.11}$$

By assuming that there is no accumulation of charge and incorporating the conductivity into the complex permittivity term, the Maxwell equations will turn in to:

$$\nabla \times \vec{E} = -j\omega\mu\vec{H} \tag{3.12}$$

$$\nabla \times \vec{H} = j\omega\varepsilon\vec{E} \tag{3.13}$$

$$\nabla \cdot \left(\varepsilon\vec{E}\right) = 0 \tag{3.14}$$

$$\nabla \cdot \left(\mu\vec{H}\right) = 0 \tag{3.15}$$

In order to identify the wave propagation in a medium, the Maxwell equations should be solved analytically or numerically. There exist several analytical and numerical methods, which can be chosen according to the problem specifications and computational expense as shown in the Figure 3.1. As mentioned in the literature survey in chapter 2, the rigorous coupled wave analysis (RCWA) is one of the most common methods to study the periodic structures. As the Figure 3.1 also indicates, this method is fast, stable, and can be applied for diverse periodic geometries. Consequently, this method is used to predict optical properties of the structures in the present thesis.

3.2. Rigorous coupled wave analysis (RCWA)

The RCWA method is one of the most common methods to solve the Maxwell equations for the periodic geometries, and it offers a very fast and efficient solution specifically for the layered structures. However, for the structures having arbitrary geometries such as circles, it can be computationally expensive, since it divides the geometry to several staircase-like layers. Therefore, to achieve an accurate solution, the number of layers should be high enough. The method is well suited for the structures having low to moderate refractive index contrast [48]. It can be applied to the structures with dimensions having fraction of nanometers [41, 42, 49] to hundreds of micrometers [21, 22, 28, 29]. Unlike the effective medium theory (EMT), RCWA can predict the field distribution in the grating-like structures [48, 50].

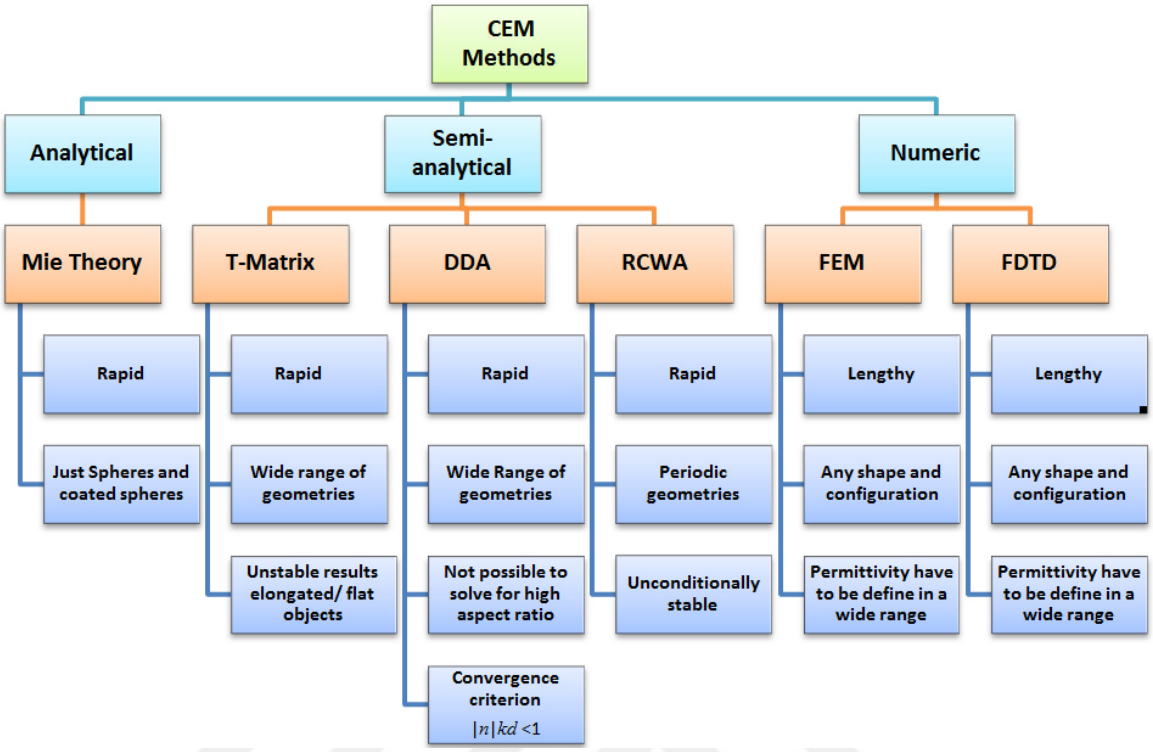


Figure 3.1. List of the methods and their specifications to solve Maxwell equations.

It is considered as a semi-analytical method as it solves the Maxwell equations in each layer analytically in the frequency domain in the longitudinal direction. In the transverse direction, the equations are solved in reciprocal space by expressing the field as a sum of spatial harmonics; by which, the partial differential equations are transformed to ordinary differential equations, which can be solved as an Eigen-value problem. While solving the ordinary differential equations, it applies Floquet's theorem to handle the periodicity of the structure.

3.3. RCWA Formulation

The Maxwell equations (Equations 3.12, and 3.13) can be represented as following by considering $\mu = \mu_0\mu_r$ and $\varepsilon = \varepsilon_0\varepsilon_r$ [48],

$$\nabla \times \vec{E} = -j\omega\mu_0\mu_r\vec{H} \tag{3.16}$$

$$\nabla \times \vec{H} = j\omega\varepsilon_0\varepsilon_r\vec{E} \tag{3.17}$$

where, μ_0 and μ_r are permeability constant and relative permeability, respectively; and ε_0 and ε_r are vacuum permittivity and relative permittivity, respectively. The Eq. 3.17 can be simplified by normalizing using the following equation:

$$\vec{\tilde{H}} = -j\sqrt{\frac{\mu_0}{\varepsilon_0}}\vec{H} \tag{3.18}$$

Therefore the Maxwell equations will be,

$$\nabla \times \vec{E} = k_0\mu_r\vec{\tilde{H}} \tag{3.19}$$

$$\nabla \times \vec{\tilde{H}} = k_0\varepsilon_r\vec{E} \tag{3.20}$$

where, k_0 is the wavenumber. By expanding these equations, the following components can be derived,

$$\frac{\partial E_z}{\partial y} - \frac{\partial E_y}{\partial z} = k_0\mu_r\tilde{H}_x \tag{3.21}$$

$$\frac{\partial E_x}{\partial z} - \frac{\partial E_z}{\partial x} = k_0\mu_r\tilde{H}_y \tag{3.22}$$

$$\frac{\partial E_y}{\partial x} - \frac{\partial E_x}{\partial y} = k_0\mu_r\tilde{H}_z \tag{3.23}$$

$$\frac{\partial \tilde{H}_z}{\partial y} - \frac{\partial \tilde{H}_y}{\partial z} = k_0\varepsilon_r E_x \tag{3.24}$$

$$\frac{\partial \tilde{H}_x}{\partial z} - \frac{\partial \tilde{H}_z}{\partial x} = k_0\varepsilon_r E_y \tag{3.25}$$

$$\frac{\partial \tilde{H}_y}{\partial x} - \frac{\partial \tilde{H}_x}{\partial y} = k_0\varepsilon_r E_z \tag{3.26}$$

For the periodic fields, the Fourier series expansion for the i^{th} layer reads as,

$$\vec{E}_i(x,y,z) = \sum_{m=-\infty}^{+\infty}\sum_{n=-\infty}^{+\infty} \vec{S}_{i,m,n}(z)\exp\left[-j(k_{m.n}^x x + k_{m.n}^y y)\right] \tag{3.27}$$

$$\vec{\tilde{H}}_i(x,y,z) = \sum_{m=-\infty}^{+\infty}\sum_{n=-\infty}^{+\infty} \vec{U}_{i,m,n}(z)\exp\left[-j(k_{m.n}^x x + k_{m.n}^y y)\right] \tag{3.28}$$

where, for a single period the wave vectors can be represented as the reciprocal lattice vectors $\vec{G}_1$ and $\vec{G}_2$ as the following,

$$k_{m,n}^x = k_{inc}^x - (m\vec{G}_1 + n\vec{G}_2)\cdot\hat{x} \tag{3.29}$$

$$k_{m,n}^y = k_{inc}^y - (m\vec{G}_1 + n\vec{G}_2)\cdot\hat{y} \tag{3.30}$$

$$k_{i,m,n}^z = \begin{cases} \sqrt{k_0^2 - \left(k_{m,n}^x\right)^2 - \left(k_{m,n}^y\right)^2} & k_0^2\varepsilon_i > \left(k_{m,n}^x\right)^2 + \left(k_{m,n}^y\right)^2 \\ -j\sqrt{\left(k_{m,n}^x\right)^2 + \left(k_{m,n}^y\right)^2 - k_0^2\varepsilon_i} & k_0^2\varepsilon_i < \left(k_{m,n}^x\right)^2 + \left(k_{m,n}^y\right)^2 \end{cases} \tag{3.31}$$

The Fourier series expansion of the permittivity and permeability functions can also be written as,

$$\varepsilon_i(x,y) = \sum_{m=-\infty}^{+\infty}\sum_{n=-\infty}^{+\infty} a_{i,m,n}\exp(j\vec{G}_{m,n}\cdot\vec{r}) \tag{3.32}$$

$$\mu_i(x,y) = \sum_{m=-\infty}^{+\infty}\sum_{n=-\infty}^{+\infty} c_{i,m,n}\exp(j\vec{G}_{m,n}\cdot\vec{r}) \tag{3.33}$$

To improve convergence, Fourier series expansions are also computed for the inverse of the permittivity and permeability as the following,

$$\varepsilon_i^{-1}(x,y) = \sum_{m=-\infty}^{+\infty}\sum_{n=-\infty}^{+\infty} b_{i,m,n}\exp(j\vec{G}_{m,n}\cdot\vec{r}) \tag{3.34}$$

$$\mu_i^{-1}(x,y) = \sum_{m=-\infty}^{+\infty}\sum_{n=-\infty}^{+\infty} d_{i,m,n}\exp(j\vec{G}_{m,n}\cdot\vec{r}) \tag{3.35}$$

where,

$$a_{i,m,n} = \frac{1}{A}\iint_A \varepsilon_i(x,y)\exp(-j\vec{G}_{m,n}\cdot\vec{r})dA \tag{3.36}$$

$$b_{i,m,n} = \frac{1}{A}\iint_A \mu_i(x,y)\exp(-j\vec{G}_{m,n}\cdot\vec{r})dA \tag{3.37}$$

$$c_{i,m,n} = \frac{1}{A}\iint_A \varepsilon_i^{-1}(x,y)\exp(-j\vec{G}_{m,n}\cdot\vec{r})dA \tag{3.38}$$

$$d_{i,m,n} = \frac{1}{A}\iint_A \mu_i^{-1}(x,y)\exp(-j\vec{G}_{m,n}\cdot\vec{r})dA \tag{3.39}$$

By substituting the presented Fourier series expansion formulas into the Maxwell equations (Equations 3.21-3.26), the equations can be transformed into the reciprocal space. While similar operations need to be done for all the Equations 3.21-3.26, only the operations on Equation 3.21 is shown in this section. The rest can be done similarly.

$$\begin{aligned}
&\tfrac{\partial}{\partial y}\sum_{m=-\infty}^{+\infty}\sum_{n=-\infty}^{+\infty} S^z_{i,m,n}(z)\exp\left[-j(k^x_{m.n}x+k^y_{m.n}y)\right]- \\
&\qquad\qquad \tfrac{\partial}{\partial z}\sum_{m=-\infty}^{+\infty}\sum_{n=-\infty}^{+\infty} S^y_{i,m,n}(z)\exp\left[-j(k^x_{m.n}x+k^y_{m.n}y)\right] \\
&= k_0\left[\sum_{m=-\infty}^{+\infty}\sum_{n=-\infty}^{+\infty} c_{i,m,n}\exp\left[j\left(mG_{x1}+nG_{x2}\right)\right]\right] \\
&\qquad\qquad \left[\sum_{m=-\infty}^{+\infty}\sum_{n=-\infty}^{+\infty} U^x_{i,m,n}(z)\exp\left[-j(k^x_{m.n}x+k^y_{m.n}y)\right]\right]
\end{aligned} \tag{3.40}$$

which can be simplified as,

$$\begin{aligned}
&\sum_{m=-\infty}^{+\infty}\sum_{n=-\infty}^{+\infty} -jk^y_n S^z_{i,m,n}(z)\exp\left[-j(k^x_{m.n}x+k^y_{m.n}y)\right] \\
&\qquad\qquad -\sum_{m=-\infty}^{+\infty}\sum_{n=-\infty}^{+\infty}\tfrac{dS^y_{i,m,n}(z)}{dz}\exp\left[-j(k^x_{m.n}x+k^y_{m.n}y)\right] \\
&= k_0\sum_{m=-\infty}^{+\infty}\sum_{n=-\infty}^{+\infty}\left[\exp\left[-j\left(k^x_{m,n}x+k^y_{m,n}y\right)\right]\sum_{q=-\infty}^{+\infty}\sum_{r=-\infty}^{+\infty} c_{i,m-q,n-r}U^x_{i,q,r}(z)\right]
\end{aligned} \tag{3.41}$$

As can be seen, and also mentioned earlier, the partial differential equation is turned to ordinary differential equation. From the Equation 3.41, there are infinite set of equations for an infinite set of spatial harmonics. For $(m,n)^{th}$ spatial harmonic, the

following equation can be represented,

$$-jk^{y}_{m,n}S^{z}_{i,m,n}(z) - \frac{dS^{y}_{i,m,n}(z)}{dz} = k_0 \sum_{q=-\infty}^{+\infty} \sum_{r=-\infty}^{+\infty} c_{i,m-q,n-r} U^{x}_{i,q,r}(z) \tag{3.42}$$

After applying similar operations for Equations 3.22-3.26 and knowing the fact that the double summation on the right hand side represents the convolution of μ_i and U^x_i, the final form of the Maxwell equations read,

$$-jk^{y}_{m,n}S^{z}_{i,m,n}(z) - \frac{dS^{y}_{i,m,n}(z)}{dz} = k_0 \mu^{x}_{i} * U^{x}_{i}(z) \tag{3.43}$$

$$\frac{dS^{x}_{i,m,n}(z)}{dz} + jk^{x}_{m,n}S^{z}_{i,m,n}(z) = k_0 \mu^{y}_{i} * U^{y}_{i}(z) \tag{3.44}$$

$$jk^{x}_{m,n}S^{y}_{i,m,n}(z) + jk^{y}_{m,n}S^{x}_{i,m,n}(z) = k_0 \mu^{z}_{i} * U^{z}_{i}(z) \tag{3.45}$$

$$-jk^{y}_{m,n}U^{z}_{i,m,n}(z) - \frac{dU^{y}_{i,m,n}(z)}{dz} = k_0 \varepsilon^{x}_{i} * S^{x}_{i}(z) \tag{3.46}$$

$$\frac{dU^{x}_{i,m,n}(z)}{dz} + jk^{x}_{m,n}U^{z}_{i,m,n}(z) = k_0 \varepsilon^{y}_{i} * S^{y}_{i}(z) \tag{3.47}$$

$$jk^{x}_{m,n}U^{y}_{i,m,n}(z) + jk^{y}_{m,n}U^{x}_{i,m,n}(z) = k_0 \varepsilon^{z}_{i} * S^{z}_{i}(z) \tag{3.48}$$

The derived formulas can then be discretized and solved numerically. In the present study the RCWA model developed as an open source MATLAB^{TM} code by Kwiecien, based on the methods introduced in [51–54], is used.

3.4. Verification studies

The model used in this study is first verified using the problem and results presented in Mao and Ye [6] as shown in Figure 3.2. In this study, a Si/SiO_2 based multilayered structure is considered, as shown in the Figure 3.2a with $d_{Si} = 0.17\mu m$, $d_{SiO_2} = 0.39\mu m$, and the calculated spectral transmittance is shown in Figure 3.2b. Good agreement can be observed between the results of the present study and the results of Mao and Ye, verifying the model used in this study, as shown in the figure.

The structure suggested by Wan [14] is considered for the second verification study. Wan modelled a W rectangular grating shown in the Figure 3.3(a) with $a_0 =$

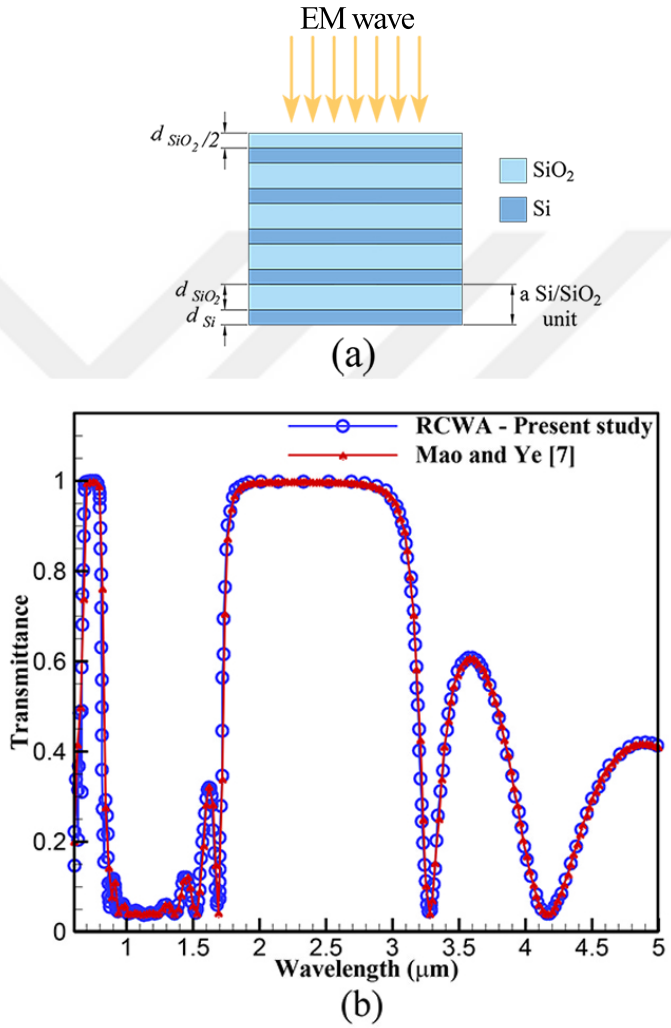


Figure 3.2. (a)The Multilayered Si/SiO_2 structure considered by Mao and Ye [6], with $d_{Si} = 0.17\mu m$, $d_{SiO_2} = 0.39\mu m$ (b) Transmittance with respect to the wavelength for RCWA code used in the present study and The results of Mao and Ye.

$1\mu m$, $d = 0.5\mu m$, $h = 0.5\mu m$, and $b = 0.3\mu m$. As the Figure 3.3(b) shows the absorptance spectrum of the structure calculated in this study and the results of Wan are in good agreement, verifying our model.

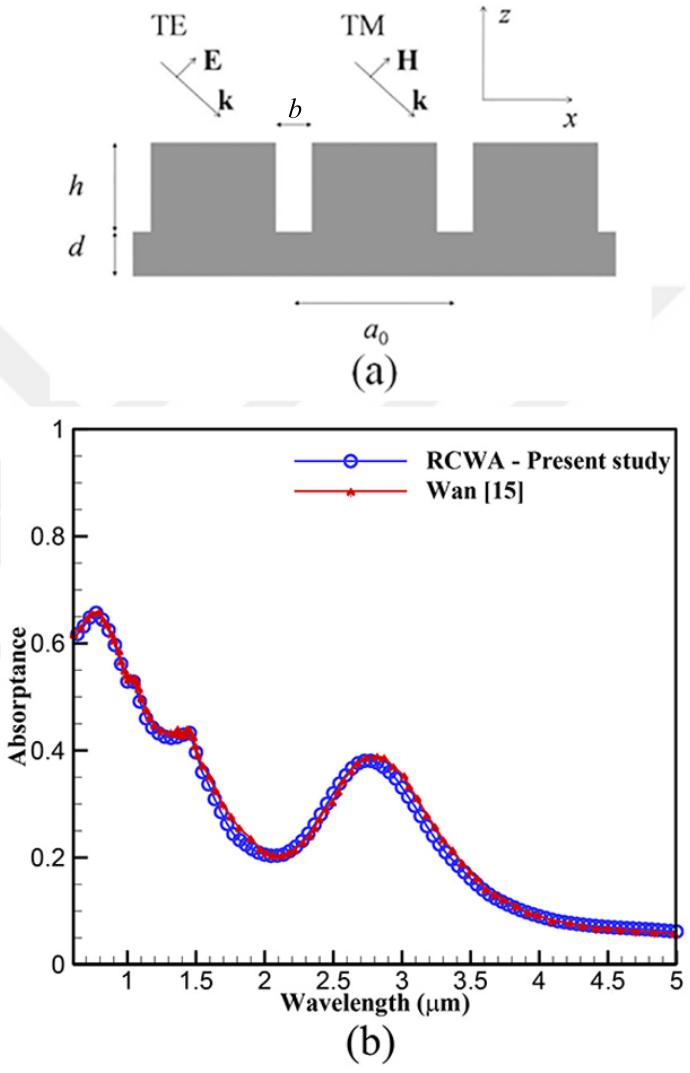


Figure 3.3. (a) The W rectangular grating suggested by Wan [14], (b) Absorptance with respect to the wavelength for RCWA code used in the present study and The results of Wan ($a_0 = 1\mu m$, $d = 0.5\mu m$, $h = 0.5\mu m$, and $b = 0.3\mu m$).

4. DESCRIPTION OF A TPV SYSTEM

A TPV system used for generation of electrical energy from a high temperature source is considered in this study. The high temperature source considered is from industrial thermal processing systems used in steel, aluminum, or glass industries. The efficiency of such systems can be maximized not only by minimizing input and waste heat, but also by utilizing the waste heat. The TPV is used to recover the heat lost by the high temperature system, and a filter is to be designed to maximize the system efficiency as shown in Figure 4.1. The efficiency of such a system can be defined as,

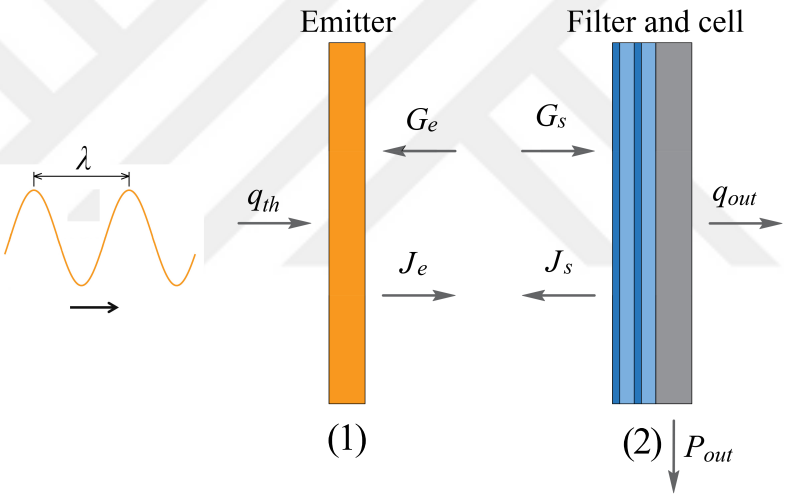


Figure 4.1. Schematic of the TPV system considered.

$$\eta = \frac{P_{out}}{q_{th}} \tag{4.1}$$

where P_{out} is the electrical power produced by the TPV and q_{th} is the heat provided by an external source to sustain the high temperature of the system. For the 1D problem considered, the high temperature system can be assumed as a blackbody emitter. While a filter is attached to the TPV cell facing the emitter, a cooling system is attached to the other side to keep its operation safe and efficient. The cooling system performance

is utilized in terms of a heat transfer coefficient, h_c, that is defined with respect to the ambient temperature, T_a.

4.1. 1D Multilayer Si/SiO_2 Photonic Crystals

A 1D multilayer photonic crystal composed of Si/SiO_2 units is a quarter-wave periodic structure like shown as (2) in Figure 4.1. Such structures can enhance the interference of the entered beam and therefore, the beam is highly transmitted or reflected. According to the quarter-wave theory, the central wavelength of the band-gap (λ_0) can be obtained from [6]:

$$\lambda_0 = \lambda_1 \left(1 + \left[\frac{2}{\pi}\sin^{-1}\left(\frac{n_{Si} - n_{SiO_2}}{n_{Si} + n_{SiO_2}}\right)\right]\right) \tag{4.2}$$

where n_{Si} and n_{SiO_2} are refractive indices of the Si and SiO_2, respectively, and λ_1 is the wavelength of the lower edge of the first stop-band of the filter and it should be chosen according to the band-gap wavelength of the TPV. Then the thickness of the Si and SiO_2 layers in each unit can be calculated by

$$d_{Si} = \frac{\lambda_0}{4n_{Si}} \tag{4.3}$$

$$d_{SiO_2} = \frac{\lambda_0}{4n_{SiO_2}} \tag{4.4}$$

Therefore, the thicknesses of the dielectric layers leading to a particular λ_1, can be explicitly expressed by considering Equations 4.2-4.4.

4.2. Thermal modeling of a thermophotovoltaic system

For steady operation, energy balance equations for emitter and the filter/cell structure can be written, respectively, as (see Figure 4.1):

$$q_{th} + G_e = J_e \;\rightarrow\; q_{th} + [\tau_f E_{b,c}(T_s) + 0.5\varepsilon_f E_{b,f}(T_s)] = E_{b,e}(T_e) \tag{4.5}$$

$$G_s = q_{out} + J_s \;\rightarrow\; E_{b,e}(T_e) = q_{out} + [\tau_f E_{b,c}(T_s) + 0.5\varepsilon_f E_{b,f}(T_s)] \tag{4.6}$$

Here, G_e and G_s are irradiation to the emitter and the filter/cell structure, respectively; J_e and J_s are the radiosity of the emitter and the filter/cell structure, respectively; $E_{b,e}(T_e)$ and $E_{b,f}(T_s)$ are the black body emissive power of the emitter and the filter at temperatures T_e and T_s, respectively, and can be calculated using Planck's law. Since there is applied voltage across the cell, the black body emissive power of the cell, $E_{b,c}(T_s)$, can be obtained by the generalized Planck's law

$$E_{b,c}(T_s) = \int_0^{\lambda_g} \frac{2\pi hc^2}{\lambda^5 \left[\exp\left(\frac{hc/\lambda - eV_{\max}}{k_b T_s}\right) - 1\right]} d\lambda \tag{4.7}$$

where, c is the speed of light in vacuum, h is the Planck's constant, k_b is the Boltzmann's constant, V_{max} is the voltage across the cell at maximum power point, e is the electron charge, and λ_g is the band-gap wavelength of the cell. Zhai *et al.* [55] proposed that the V_{max} can be calculated as:

$$V_{\max} = \frac{hc}{e\lambda_g}\left(1 - \frac{T_s}{T_e}\right) \tag{4.8}$$

In Equations 4.5 and 4.6, τ_f is the transmittance of the filter, and ε_f is the emittance of the filter, which is equal to the absorptance (α_f). In Equations 4.5 and 4.6, 0.5 factor is introduced as only half of the emissive power radiated from filter reaches the emitter, since the filter is attached with PV cell on the right side and the emission from the right side is absorbed by the cell. The final equation must consider the energy balance over the cell including the convective cooling boundary condition as

$$q_{out} = P_{out} + h_c(T_s - T_a) \tag{4.9}$$

where, h_c is the convective heat transfer coefficient, and T_a is the ambient temperature. Then, the output electrical power (P_{out}) can be predicted through an iterative solution of the non-linear set of Equations 4.5-4.9.

4.3. Detailed balance principle and fundamental losses in photovoltaic devices

Detailed balance principle of photovoltaic cells was proposed by the Shockley and Queisser [56] in 1961, and it can be used to estimate the maximum efficiency of the photovoltaic devices. It is based on the generalized Planck's equation to calculate the photocurrent generated in the cell by the following formula:

$$J = e(\phi_{abs} - \phi_{emit}) \tag{4.10}$$

where, ϕ_{abs} and ϕ_{emit} are the absorbed and emitted photon flux by the cell that can be calculated by the generalized Planck's equations:

$$\phi_{abs} = \int_0^{\lambda_g} \frac{2\pi c}{\lambda^4 \left[\exp\left(\frac{hc}{\lambda k_b T_e}\right) - 1\right]} \tau_{\lambda f} d\lambda \tag{4.11}$$

$$\phi_{emit} = \int_0^{\lambda_g} \frac{2\pi c}{\lambda^4 \left[\exp\left(\frac{hc/\lambda - eV}{k_b T_s}\right) - 1\right]} \tau_{\lambda f} d\lambda \tag{4.12}$$

Here, V is the applied voltage across the cell. As perfect charge transport is assumed, eV represents the chemical potential of the electron-hole pairs inside the cell. By multiplying V_{max} by current density, J, which itself is a function of V_{max}, the maximum electrical power output can be obtained

$$P_{out} = V_{\max} J(V_{\max}) \tag{4.13}$$

Table 4.1. Fundamental losses in a PV cell [57].

Above λ_g loss	$L_a = \int_{\lambda_g}^{\infty} \frac{2\pi hc^2}{\lambda^5 \left[\exp\left(hc/\lambda k_b T_e\right) - 1\right]} \tau_{\lambda f} d\lambda$	(4.14)
Thermalization loss	$L_{th} = \int_0^{\lambda_g} \frac{2\pi hc^2}{\lambda^5[\exp(hc/\lambda k_b T_e)-1]} \tau_{\lambda f} d\lambda - \int_0^{\lambda_g} \frac{2\pi hc^2/\lambda_g}{\lambda^4[\exp(hc/\lambda k_b T_e)-1]} \tau_{\lambda f} d\lambda$	(4.15)
Emission loss	$L_e = \int_0^{\lambda_g} \frac{2\pi hc^2/\lambda_g}{\lambda^4 \left[\exp\left(\frac{hc/\lambda - eV_{\max}}{k_b T_s}\right) - 1\right]} \tau_{\lambda f} d\lambda$	(4.16)
Carnot loss	$L_c = \frac{hc}{e\lambda_g} \left(\frac{T_s}{T_e}\right) J(V_{\max})$	(4.17)

Some of the fundamental losses in a TPV system [57] are introduced in the Table 4.1. The losses due to the photons radiated to the cell having energy less than the band gap energy of the cell is indicated by "Above λ_g loss", L_a (Equation 4.14). Additionally, some incoming photons have energy that is more than the band-gap energy, which can excite the carriers to interact with lattice phonons leading to thermalization losses (L_{th}) and can be calculated by Equation (4.15). Equation (4.16) represents the emission loss (L_e) due to the thermal emission of photons from the cell, and Carnot losses (L_c) are caused by the voltage drop in the cell necessary to collect the excited carriers inside the cell (Equation 4.17).

5. OPTIMIZATION OF SPECTRALLY SELECTIVE Si/SiO_2 BASED FILTERS FOR THERMOPHOTOVOLTAIC DEVICES

In this chapter, spectrally selective Si/SiO_2 based filters are designed to enhance the overall efficiency of the thermophotovoltaic devices. A methodology is developed to optimize and apply the designed filters to different types of TPV cells.

5.1. Objectives

When emitters/filters that have transparent bands within IR ranges are used with a TPV cell, the cell receives radiation above its band-gap that reduces its efficiency due to heating. Emitters/filters that exhibit successful spectral selectivity are relatively complex and hard to manufacture [13–15,17,18]. The manufacturing complexity becomes more significant when 2D structures are used; although, the spectrally selective behavior is improved in comparison to the 1D structures. Complexity rises due to the larger number of processes that have to be applied in order to manufacture a 2D structure [6]. It can also be noted that, using diverse materials in a single structure, adds another challenge to manufacturing process and the number of process increases further [6]. Therefore, a multilayered 1D structure that has superior performance is designed in this study in order to overcome the mentioned issues. Moreover, Si and SiO_2 are the materials that are widely used in diverse fields of nano-technology due to their distinct specifications, low cost, and precise manufacturing methods for these materials are well established. However, the studied 1D Si/SiO_2 based filters transmit well in below band-gap wavelengths, there also exist some undesired transmittance at above band-gap wavelengths, which can cause reduction in overall efficiency of the TPV cell [5–7]. Therefore, further improvements should be implemented to avoid undesired transmittance. The present study outlines a design methodology for such devices and focuses on designing simple 1D Si and SiO_2 multilayers to filter out the unwanted band-gap radiation. Accordingly, spectrally selective behavior can be achieved by using a low

cost, easy to manufacture system. In this paper, an optimized Si/SiO_2 based structure is proposed, which successfully reflects wider range of above band-gap wavelengths in comparison to the cases studied in [5–7] which enhance the overall efficiency of the TPV device.

5.2. Methodology

RCWA is used in order to estimate the transmittance of the designed filter as discussed in chapter 3. Genetic Algorithm (GA) methodology, that is a global optimization method [58] is used by defining the objective function as the overall efficiency of the system, η, in order to optimize the parameters of the designed filter to approach the ideal case. GA mimics the natural selection process inspired by Darwinian biological evolution. This method initialized by selection of the individuals randomly distributed in the population prescribed by constrains of the optimization parameters. Then, according to the fitness function, the best fitted solutions are selected and are considered as parents for the next generation. This process progresses until the optimal solution is achieved according to the stopping criteria. In the present study, the GA implementation of the global optimization toolbox of the MATLAB^{TM} is utilized to find optimized λ_1's for the filters that maximize the efficiency, η, considered as the fitness function. The number of generation is set to be 200 with stopping criteria as 10^{-4}, which leads to acceptable results.

5.3. Results and discussion for Si/SiO_2 based multilayered structures

5.3.1. Filter design

In this study, a number of filter designs based on Si and SiO_2 layers are considered. First, the structure suggested by Mao and Ye [6], presented in Figure 5.1(a) (design 1) is explained. This filter is composed of five Si/SiO_2 units for GaSb based PV cell. The same concept is also adopted for InGaSb based PV cell by changing the λ_1 according to the band-gap of the cell. Since InGaSb has a band-gap wavelength of $\lambda_g = 2.21\mu m$, the first stop-band wavelength is chosen to be $\lambda_1 = \lambda_g = 2.21\mu m$.

The refractive indices of the Si and SiO_2 are considered as $n_{Si} = 3.4$, $n_{SiO_2} = 1.5$, respectively, for estimation of layer thicknesses using the Equations 4.2-4.4. However, in transmittance calculations, the spectral refractive and absorptive indices of both materials as shown in Figures 5.2 and 5.3 is considered [59]. While the thicknesses are estimated as $d_{Si} = 0.204\mu m$ and $d_{SiO_2} = 0.462\mu m$, the thickness of the first SiO_2 layer is taken as $d_{SiO_2}/2$ as shown in the Figure 5.1(a) in order to achieve an anti-reflection effect [6].

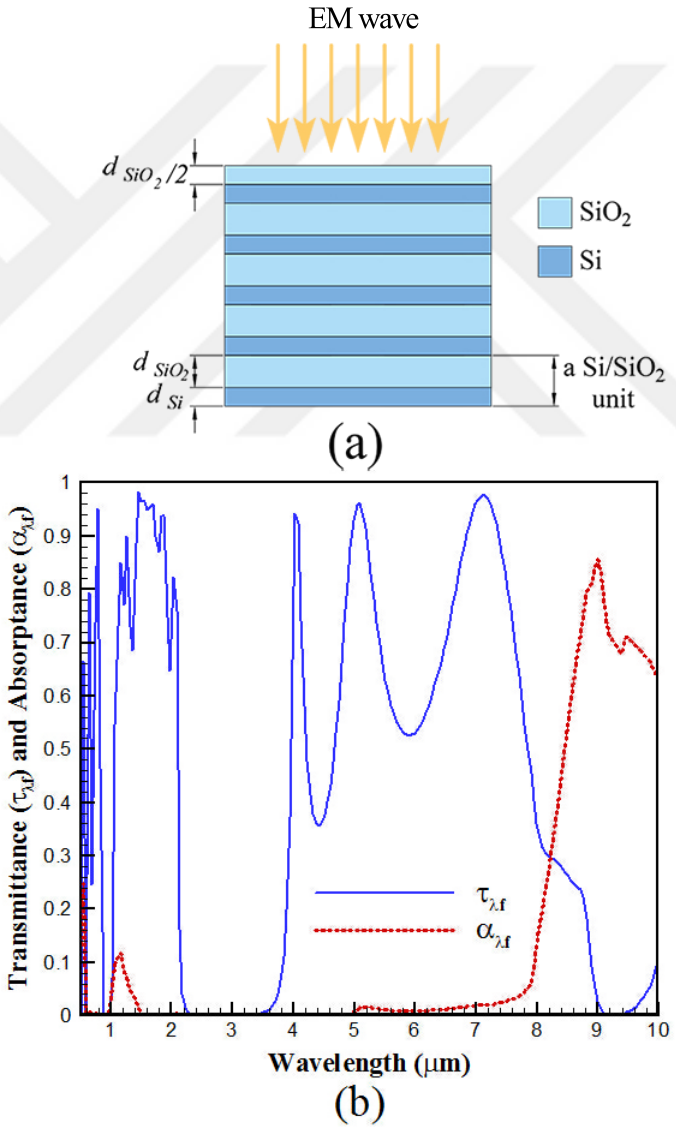


Figure 5.1. (a) 10 layered structure with five Si/SiO_2 units (design 1), (b) transmittance and absorptance spectrum of design 1 structure.

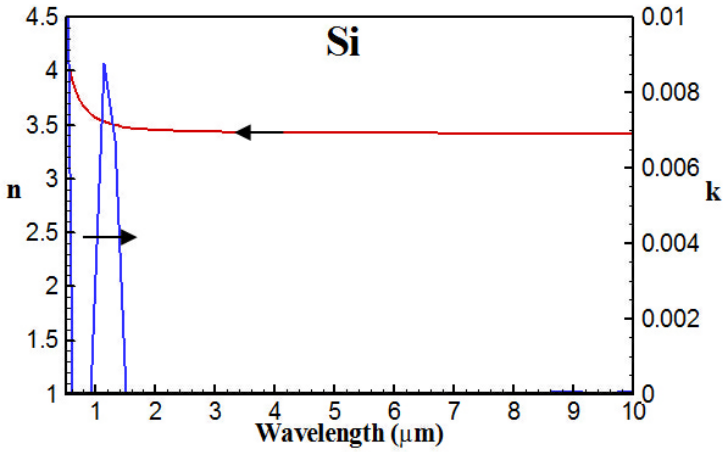


Figure 5.2. Refractive index of Si [59].

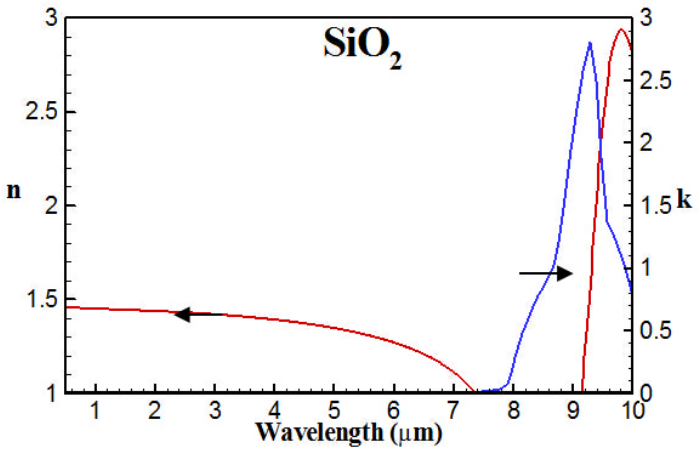


Figure 5.3. Refractive index of SiO_2 [59].

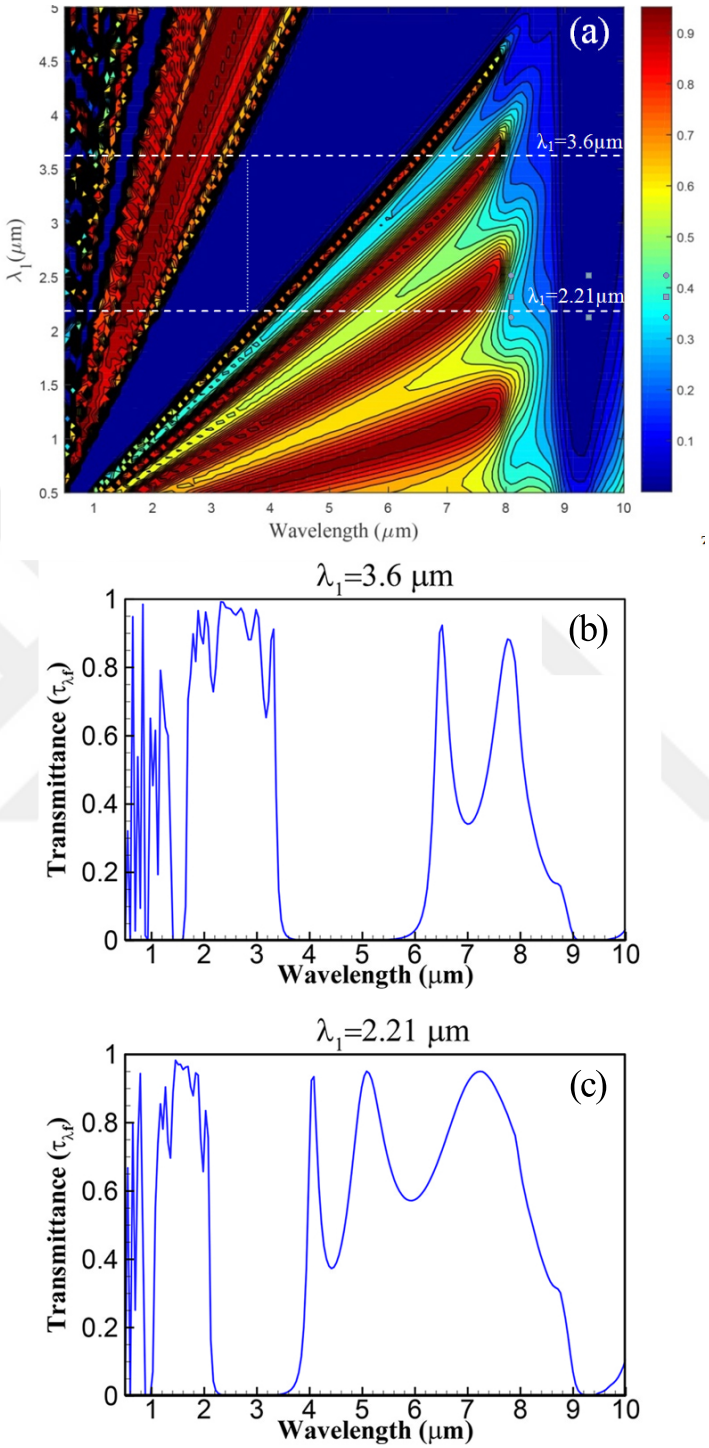


Figure 5.4. (a) Transmittance contour plot of the structure with five Si/SiO_2 units (design 1) when λ_1 is changing, (b) transmittance with $\lambda_1 = 3.6\mu m$, (c) transmittance with $\lambda_1 = 2.21\mu m$.

The spectral transmittance and absorptance of the considered structure for normal incidence is presented in Figure 5.1(b). It can be observed that the structure reflects almost all radiation between $2.21 - 3.5\mu m$, while it slightly absorbs between $1 - 1.5\mu m$. At $0.5\mu m$ the absorptance becomes significant, and it reaches a value of 80% for wavelengths above $8\mu m$. While high transmittance bands are observed beyond $3.5\mu m$, the incoming radiation in this range is not convertible to the electricity and would increase the temperature of the cell and then reduce the efficiency of the system; therefore, must be avoided. The transmittance behavior of the structure for changing λ_1 that is presented in Figure 5.4(a) should be considered in order to find a solution to this issue.

It can be observed that for $\lambda_1 = 2.21\mu m$ (marked by bottom white dashed line), there is some unwanted transmittance for the wavelengths higher than $3.6\mu m$ as mentioned above also be seen in Figure 5.4(c). The contour suggests that using another similar structure attached on top of the considered structure with $\lambda_1 \approx 3.6\mu m$ (marked by top white dashed line) it would be possible to filter out the majority of the unwanted radiation. The transmittance of the top structure with $\lambda_1 = 3.6\mu m$ is shown in Figure 5.4(b). The structure shown in Figure 5.5(a) is proposed based on this concept. In this structure, which is named as Design 2, the bottom Si/SiO_2 set (set 1) is identical to the previous structure (Design 1). However, another set of Si/SiO_2 with different λ_1 is added on top of the Design 1.

However, in order to filter out the transmittance in higher wavelengths, another similar structure, but with greater λ_1 is attached to emitter side of the filter. By selecting λ_1's for the two Si/SiO_2 sets, as shown in Figure 5.5(a), overall efficiency of the TPV system operating with InGaSb cell can be maximized. Global optimization is utilized considering the overall efficiency as the objective function and λ_1's for the two sets being unknown design parameters. The corresponding layer thicknesses of the optimal design can then be directly estimated from these two first stop wavelengths. The optimization considering, $T_e = 1800K$, and $T_a = 300K$ led to $\lambda_1 = 2.218\mu m$ for the bottom set (set 1), and $\lambda_1 = 3.643\mu m$ for the top set (set 2) as shown in Figure 5.5(a). The corresponding thicknesses are estimated as $d_{SiO_2,1} = 0.462\mu m$, and

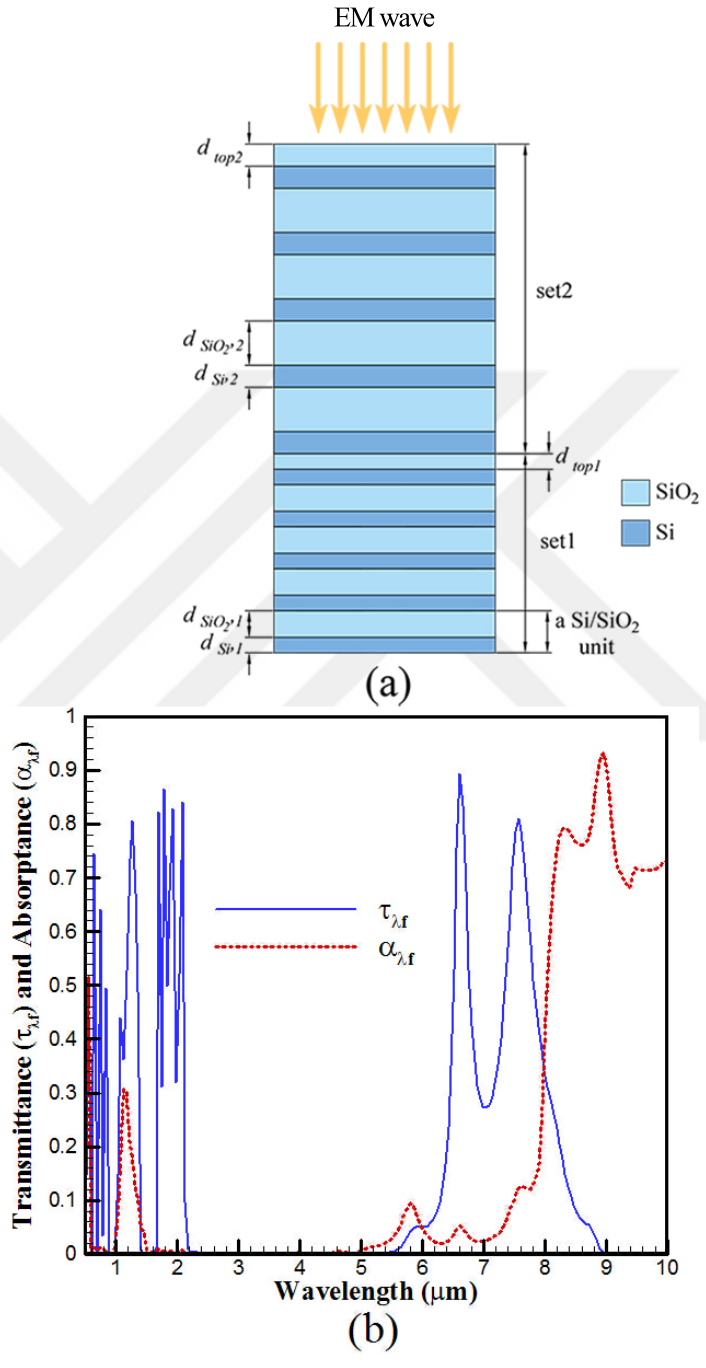


Figure 5.5. (a) 20 layered structure with two sets of five Si/SiO_2 units (Design 2), (b)Transmittance and absorptance spectrum of Design 2.

$d_{Si,1} = 0.204\mu m$, $d_{SiO_2,2} = 0.761\mu m$, $d_{Si,2} = 0.336\mu m$. The first layers in each sets are, $d_{top1} = d_{SiO_2,1}/2$, and $d_{top2} = d_{SiO_2,2}/2$, as explained earlier. The resulting spectral transmittance and absorptance is presented in Figure 5.5(b), where it can be observed that the filter is opaque between $2.21 - 5.5\mu m$. However, between $6 - 9\mu m$ it is semi-transparent with the absorptance becoming significant beyond $8\mu m$. All the analyses are carried out up to $10\mu m$ as only less than 5% of the black-body emissive power lies beyond the $10\mu m$ in the considered emitter temperature range $(1000 - 1800K)$.

5.3.2. Performance evaluation of the filters

The performance of the suggested structure (Design 2) is evaluated for a TPV system for an emitter temperature range of $T_e = 1000 - 1800K$. The convective heat transfer coefficient representing the cooling system attached to the back of the cell is considered as $h_c = 10,000W/m^2 - K$, which can be achieved by a thermal management system relying on forced convection or phase change. Thermal contact resistances are neglected and filter is considered as lumped due to the small radiative Biot number ($Bi = \sigma T_s^3 d_{tot}/k_f$), considering the filter temperature, $T_s = 340K$ for the highest temperature case, the total thickness of the filter, $d_{tot} = 8.2\mu m$ for the thickest filter used (Design 2), and the effective thermal conductivity of the filter, k_f is calculated to be $2.07W/m-K$ with thermal conductivity of the Si and SiO_2 considered as $149W/m-K$ and $1.4W/m-K$, respectively [60]. The temperature dependent band-gap wavelength of the InGaSb is derived based on the data presented by Francoeur *et al.* [61] as $\lambda_g(T_s) = 1.803 \times 10^{-3} T_s + 1.673$ in μm. The performances of the systems with proposed filters are compared with a system with no filter and a system with ideal filter. Here, the ideal filter is considered as one that transmits all radiation below band-gap wavelength and reflects the rest.

Figures 5.6 and 5.7 present the electrical power output and input power required for the system at different emitter temperatures, respectively. Although, the output power generated by the optimized filter (Design 2) is less than other cases, its efficiency is relatively higher as shown in Figure 5.8. There are two reasons of the observed high efficiency. The first one is in regards to reducing the heat required to keep emitter at

a specified temperature by reflecting the longer wavelength radiation that cannot be converted to electricity, back to the emitter. The second reason of the enhancement is due to improved cell efficiency as a result of low temperature achieved in the cell as presented in Figure 5.9.

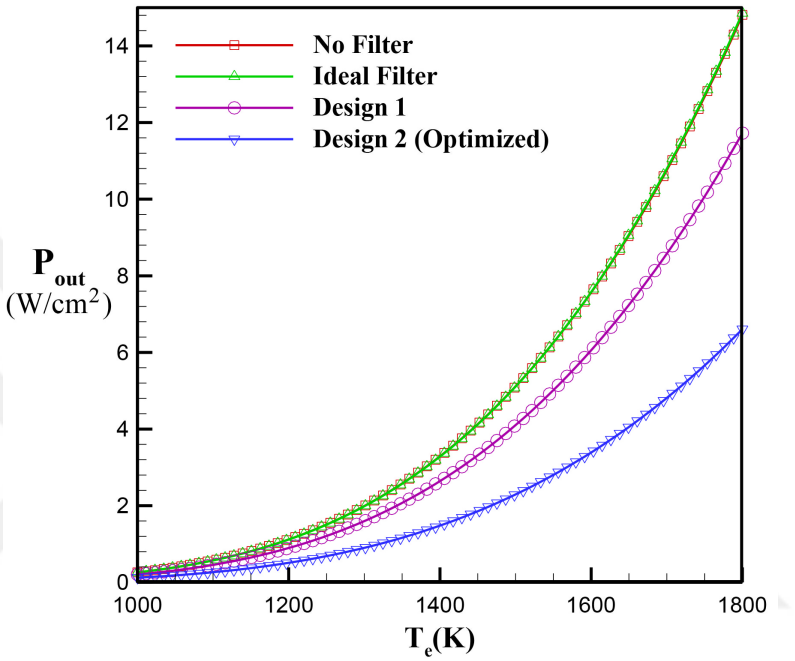


Figure 5.6. Output electrical power (P_{out}) with respect to the emitter temperature (T_e) for different filter cases.

Figure 5.10 shows the cell losses with increasing cell temperature considering an InGaSb cell for a blackbody emitter at $1800K$. In the figure the cell is considered separately so that there is no filter. The losses presented in Figure 5.10 are normalized with blackbody emissive power of the emitter. As the figure reveals, P_{out} reduces with increasing cell temperature (blue section) and the dominant energy loss is due to above band-gap incident radiation on the cell, L_a (green section), although, it is insensitive to the cell temperature. The contribution of the emission loss, L_e, (yellow section) and Carnot loss, L_c, (purple section) are less than 10% and increase as the cell temperature increases. However, the thermalization loss, L_{th}, (pink section) percentage remains constant while the cell temperature increases. Figure 5.11 shows the fundamental losses presented in Table 4.1 for different filters considered in this study for a blackbody

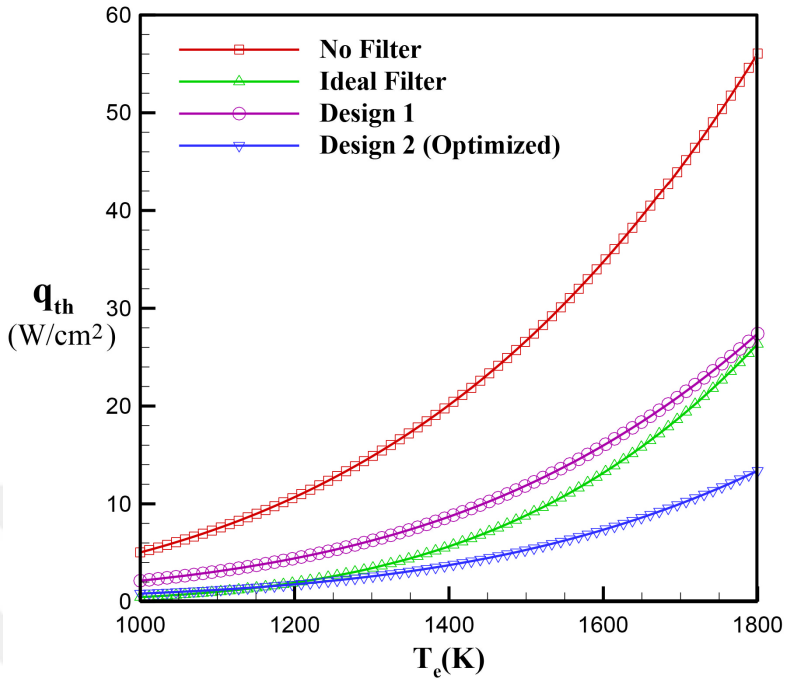


Figure 5.7. Input power to the system (q_{th}) with respect to the emitter temperature (T_e) for different filter cases.

emitter at $1800K$. The loss due to the above λ_g emission, L_a, for Design 2, is less than it is for Design 1. Whereas, the Carnot loss, L_c, and emission loss, L_e, is less than 10% in all the cases. However, it was observed that the loss due to the thermalization, L_{th}, is significant in all cases except no-filter case. The main contributor to efficiency reduction in the no-filter case is the above band-gap loss, L_a, leading to increased cell temperature that reduces efficiency.

5.3.3. Simulation of the suggested filter design in TPV devices with other cell materials

In order to show the capability of the suggested filter structure, similar analysis is carried out for different type of cells with diverse band-gap wavelengths. Si, GaSb, and $Ga_{0.78}In_{0.22}As_{0.19}Sb_{0.81}$ type cells are considered in this section. Varshni equation is

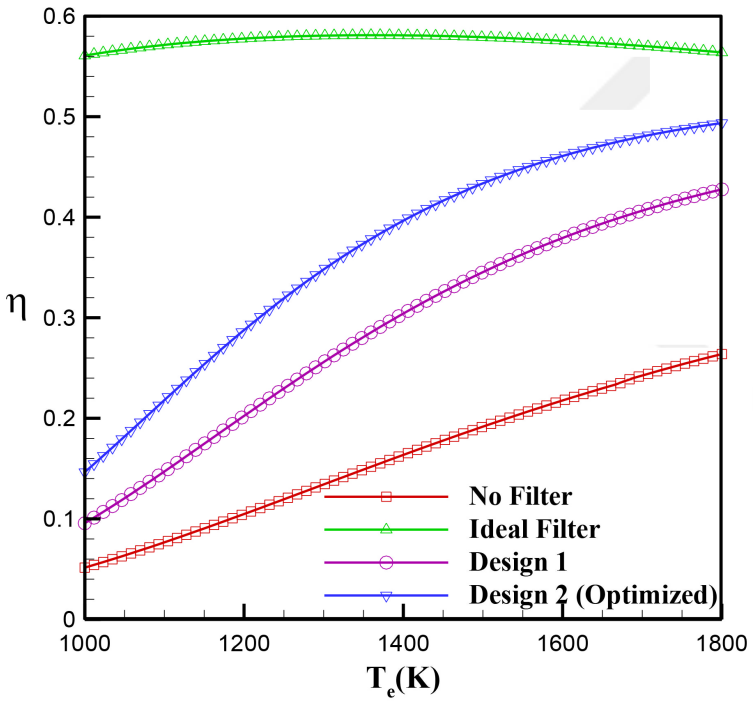


Figure 5.8. Overall efficiency (η) with respect to the emitter temperature (T_e) for different filter cases.

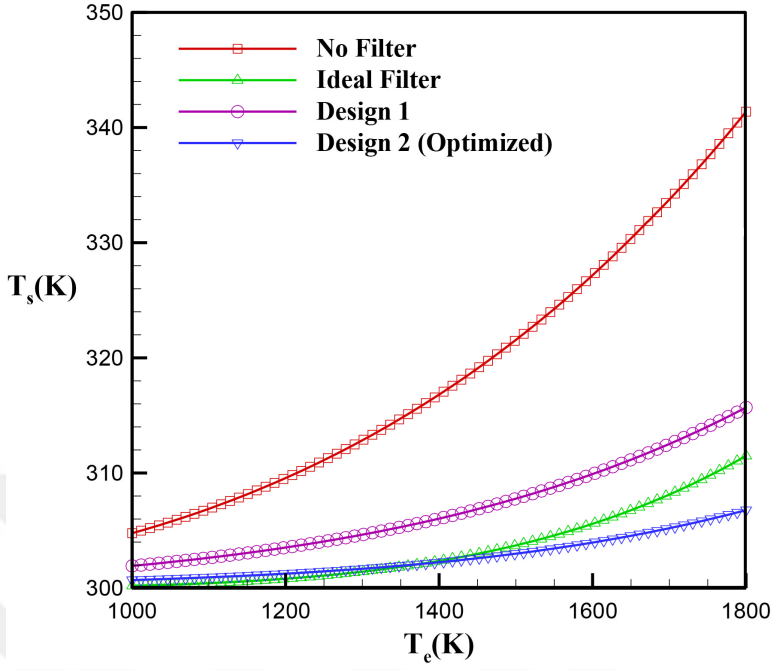


Figure 5.9. The cell temperature (T_s) with respect to the emitter temperature (T_e) for different filter cases.

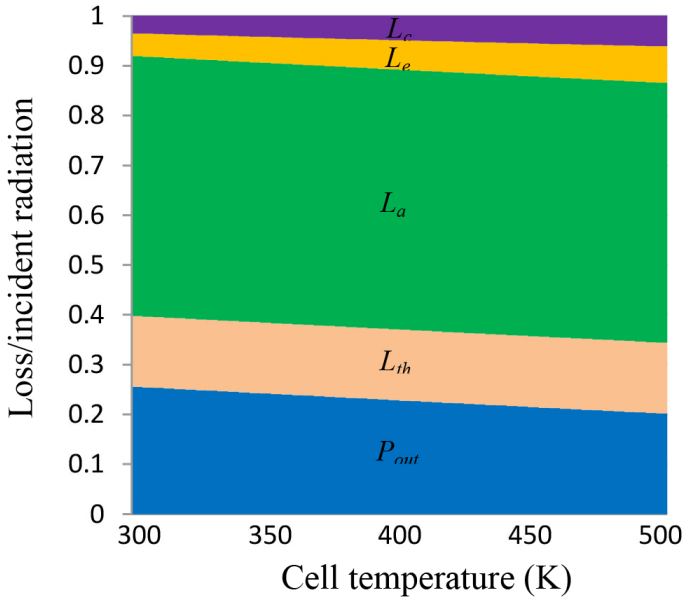


Figure 5.10. Fundamental losses and maximum electrical power output with respect to the cell temperature in the InGaSb cell for $T_e = 1800K$, normalized with incident radiation.

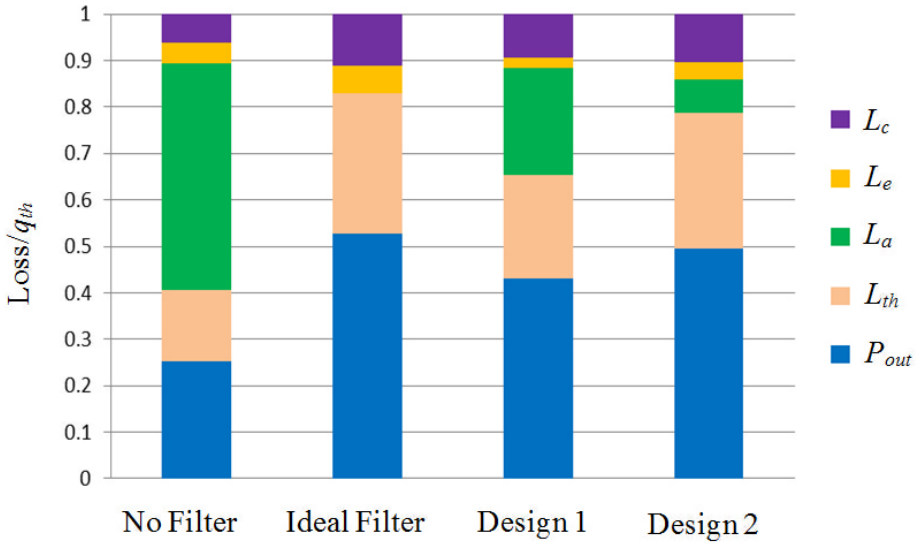


Figure 5.11. Fundamental losses and maximum electrical power output of the systems with different types of filters for $T_e = 1800K$, normalized with q_{th}.

used in order to find the temperature dependent band-gap energy of each cell type [62].

$$E_g(T_s) = E_g(0) - \frac{\alpha_E {T_s}^2}{T_s + \beta_E} \tag{5.1}$$

where, $E_g(0)$ is the band-gap energy at absolute zero, α_E and β_E are the material specific constants and they are presented in Table 5.1 for the considered materials. By optimizing for the TPV devices with these cell types similar to the case for the InGaSb cell, the estimated Si/SiO_2 layer thicknesses are listed in Table 5.2. The efficiencies of the TPV systems with respect to the emitter temperature for different cell types are also presented in Figures 5.12, 5.13, and 5.14 .

It can be observed that the system efficiency can be improved over the entire emitter temperature range by using the optimized structure (Desin 2) for all the considered cell types. For Si cell, although good enhancement is achieved by using Design 2 filter, the overall efficiency is much less than the idealistic case. Therefore, the proposed filter is not suitable to use with Si TPV cells for the considered emitter temperature range. For $Ga_{0.78}In_{0.22}As_{0.19}Sb_{0.81}$ type cell with Design 2 filter, the overall efficiency at higher

Table 5.1. Varshni equation constants for Si, GaSb, and $Ga_{0.78}In_{0.22}As_{0.19}Sb_{0.81}$.

	$E_g(0)$ (eV)	α_E (eV/K)	β_E (K)
Si [63]	1.170	$4.73e-4$	636
GaSb [30]	0.809	$5.3e-4$	234
$Ga_{0.78}In_{0.22}As_{0.19}Sb_{0.81}$ [30]	0.594	$4e-4$	290

Table 5.2. Optimized layer thicknesses for different cell types.

	$d_{Si,1}$ μm	$d_{SiO_2,1}$ μm	$d_{Si,1}$ μm	$d_{SiO_2,2}$ μm
Si	0.135	0.305	0.274	0.621
GaSb	0.206	0.466	0.370	0.839
$Ga_{0.78}In_{0.22}As_{0.19}Sb_{0.81}$	0.283	0.642	0.568	1.287

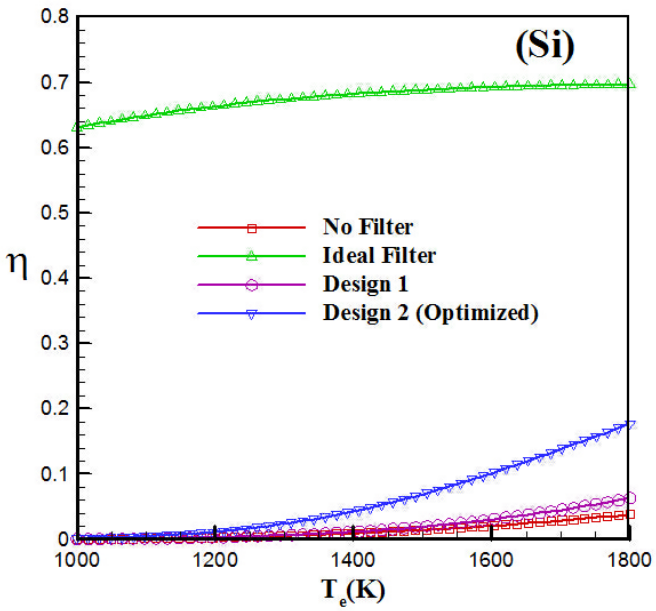


Figure 5.12. Overall efficiency (η) (see Equation 4.1) with respect to the emitter temperature (T_e) with different filter cases for Si.

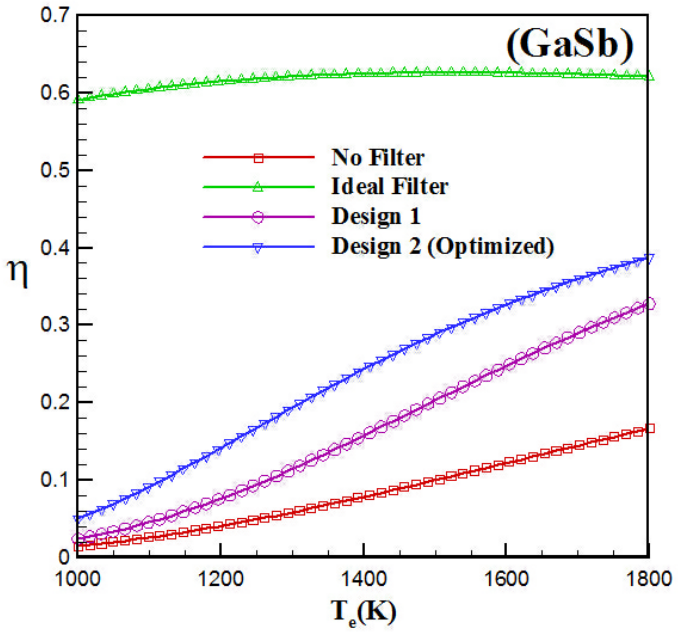


Figure 5.13. Overall efficiency (η) (see Equation 4.1) with respect to the emitter temperature (T_e) with different filter cases for GaSb.

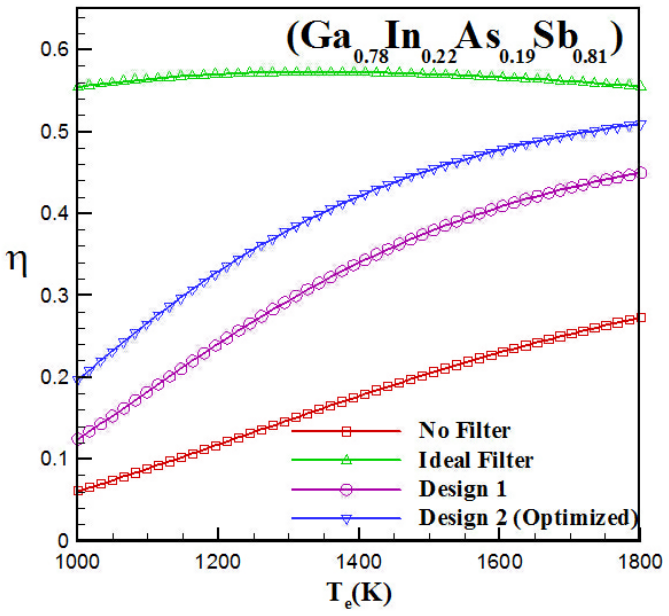


Figure 5.14. Overall efficiency (η) (see Equation 4.1) with respect to the emitter temperature (T_e) with different filter cases for $Ga_{0.78}In_{0.22}As_{0.19}Sb_{0.81}$.

temperatures is almost equal to InGaSb based TPV. However, at lower temperatures, $Ga_{0.78}In_{0.22}As_{0.19}Sb_{0.81}$ cell is more efficient than InGaSb cell. Therefore, for the considered emitter temperature range, $Ga_{0.78}In_{0.22}As_{0.19}Sb_{0.81}$ has the best performance among the presented cell types.

6. ENHANCEMENT OF SPECTRAL ABSORPTION AND TRANSMISSION OF GRAPHENE BASED NANO-STRUCTURES IN NARROW-BANDS

6.1. Objectives

As mentioned above, achieving high efficiency in energy generation by using TPV devices is a challenging issue and designing spectrally selective emitter/filters can be crucial. On the other hand, it is shown in the literature that, Gr can play a key role on designing spectrally selective emitter/filters. However, achieving a practical and relatively easy to manufacture structure with the desired spectral behavior in near-infrared wavelength range where the thermal devices such as TPV work is still an open problem that needs to be addressed. As mentioned earlier, in these devices, only the radiation at the wavelengths lower than the band-gap wavelength of the TPV cell is convertible to electricity and the radiation at higher wavelengths leads to heating of the device, reducing the efficiency. Therefore, designing an emitter or a filter emitting or transmitting at the wavelengths lower than the TPV cell band-gap wavelength is critical. In this study, two Gr based nano-structures are investigated to achieve narrow-band absorption and/or transmission. Our objective is to design these emitters so that almost monochromatic absorptance in the near-IR wavelengths can be achieved. Whereas by optimizing the geometric parameters, high transmittance is observed in a specific narrow-band range within the near-IR wavelengths for the filter applications.

6.2. Graphene-layer systems

Zhao *et al.* [42] studied Gr-based structure, whose geometry is shown in Figure 6.1(a). As clear from the absorptance spectrum in Figure 6.1(b), their system displays a narrow band high absorptance double peak. Specifically at the wavelength of $0.54\mu m$, the absorptance is 100% and it is almost monochromatic. However, the bonding the Gr having thickness of a fraction of a nm over the gaps between gratings is not practical.

In order to overcome this, a Gr layer can be coated over a Si film and the combined structure can be bonded over the Ag grating as shown in the Figure 6.2(a) (Design 3). Another alternative structure is bonding Gr coated Ag gratings over Gr coated Si layer as shown in Figure 6.2(b) (Design 4). The optical behaviors of these structures are investigated in this chapter. As the results predicted, both structures met a narrow band absorptance which can also is used as a narrow-band emitter for different applications. By changing the geometric parameters of the Design 4 structure narrow-band spectrally selective transmittance is achieved which can be applied as a filter in diverse applications such as TPV devices.

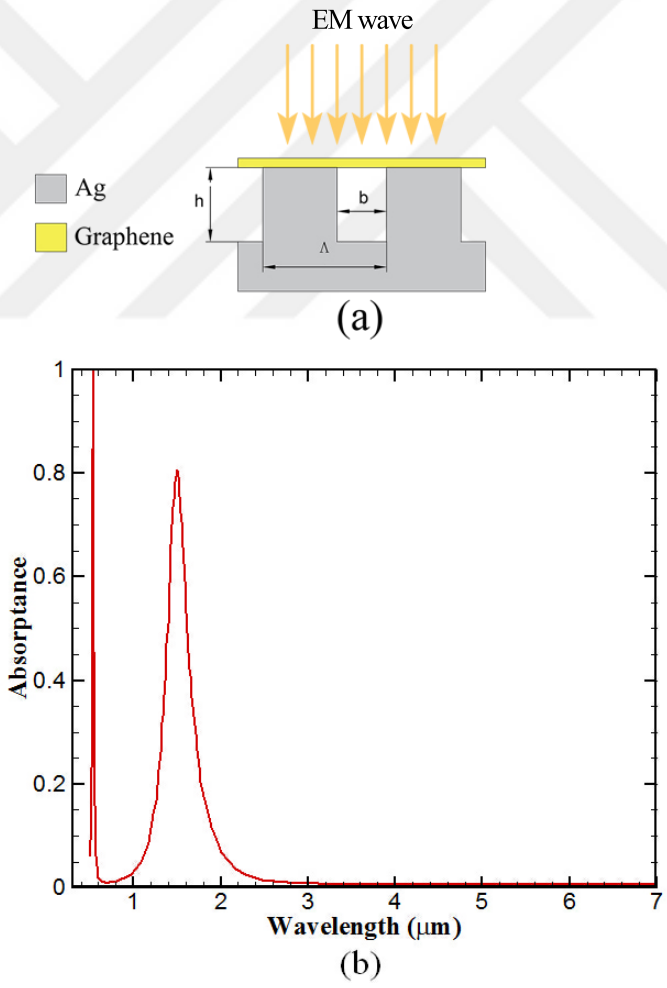


Figure 6.1. Schematic of the Ag and Gr structures considered by Zhao *et al.* [42] and absorptance spectrum.

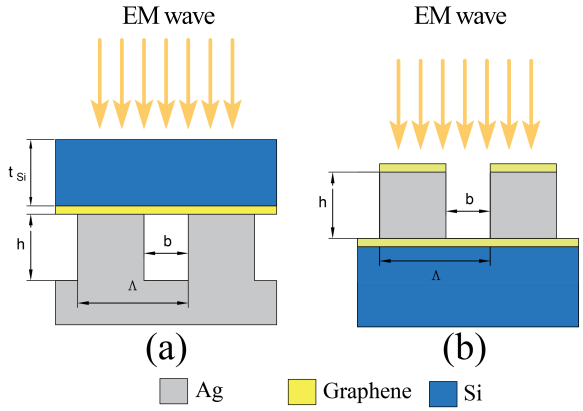


Figure 6.2. Schematic of the structures considered. Design 3(a), and Design 4(b).

The optical properties of the Gr and the Ag are estimated using Kubo formulation (Equation 6.1-6.4) and Drude model (Equation 6.5), respectively. The dielectric function of Gr can be defined as:

$$\varepsilon = \frac{i\sigma}{\varepsilon_0 \omega \Delta} \tag{6.1}$$

where, ε_0 is the vacuum permittivity and ω is the angular frequency, Δ is the thickness of Gr that is assumed to be $0.3nm$. Here σ is the sheet electrical conductance, which can be defined as $\sigma = \sigma_{Drude} + \sigma_{Inter}$. The first term is Drude part which corresponds to the intraband electron-photon scattering, and the second term deals with interband electron transitions. They can be defined as,

$$\sigma_{Drude}(\mu, \omega, T) = \frac{ie^2}{(\omega + i/\tau)\pi\hbar^2} 2k_b T \ln\left[2\cosh\left(\frac{\mu}{2k_b T}\right)\right] \tag{6.2}$$

$$\sigma_{Inter}(\mu, \omega, T) = \frac{e^2}{4\hbar^2}\left[G\left(\frac{\hbar\omega}{\pi}\right) + i\frac{4\hbar\omega}{\pi}\int_{\eta=0}^{\infty} \frac{G(\eta) - G(\hbar\omega/2)}{(\hbar\omega)^2 - 4\eta^2} d\eta\right] \tag{6.3}$$

and the function $G(\eta)$ is defined as,

$$G(\eta) = \frac{\sinh(\eta/k_bT)}{\cosh(\eta/k_bT) + \cosh(\mu/k_bT)} \tag{6.4}$$

In these equations, e is the electron charge, $\hbar$ is the reduced Planck constant, k_b is the Boltzmann constant. In this study, the values of chemical potential (μ), and relaxation time (τ), is considered as $0.3eV$, and $10 - 13s$, respectively [42]. Whereas the temperature (T) is considered as, $300K$. Drude model for silver can be presented as:

$$\varepsilon(\omega) = \varepsilon_\infty - \frac{{\omega_p}^2}{\omega(\omega - i\gamma)} \tag{6.5}$$

The Drude model parameters considered for Ag are the high frequency constant (ε_∞), plasma frequency (ω_p), and scattering rate (γ) and they are considered as 3.4, $1.39 \times 10^{16} rad/s$, and $2.7 \times 10^{13} rad/s$, respectively [49].

Both real and imaginary parts of the doped Si refractive index are considered in this study (Figure 5.2) to include the absorbing behavior of Si in the analysis [59]. Normal incidence wave with transverse magnetic (TM) polarization is considered in the analysis.

6.3. Verification study of the application of the Drude model and Kubo formula

In order to verify the application of the Drude model for Ag and Kubo formula for Gr, the RCWA code, in which the mentioned formulas are embedded, is verified with the results of Zhao *et al.* [42]. The Figure 6.3(a) shows the structure considered by Zhao *et al.* composed of an Ag grating ($h = 0.2\mu m$, $b = 0.03\mu m$, and $\Lambda = 0.4mum$) covered with a Gr layer. The Figure 6.3(b). shows the absorptance calculated in the present study and the results of Zhao *et al.* As the figure shows, good agreement is achieved

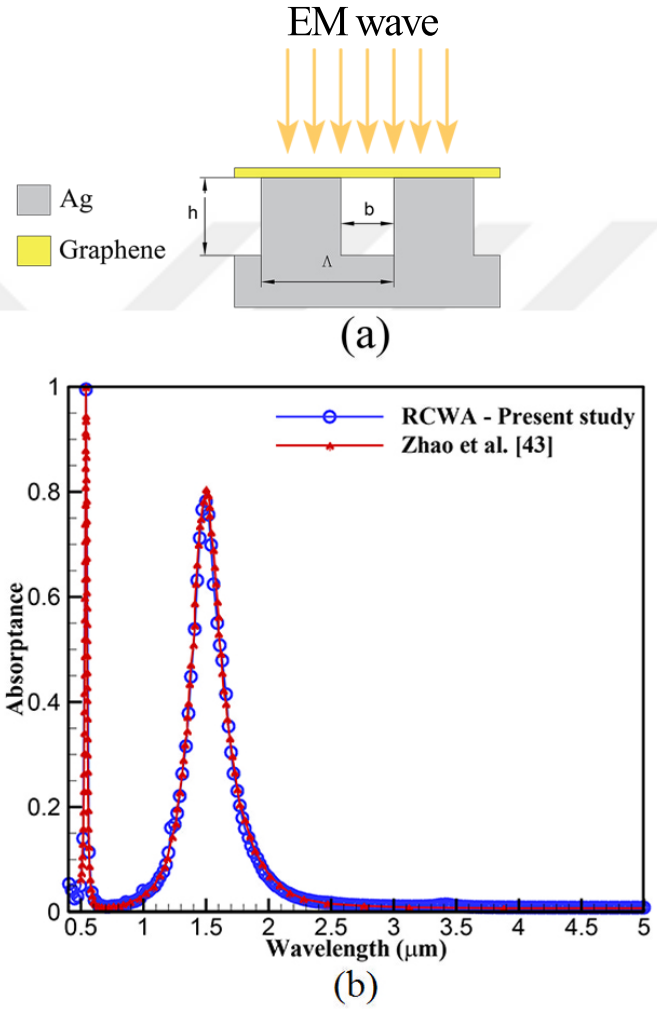


Figure 6.3. The Ag grating structure with $h = 0.2\mu m$, $b = 0.03\mu m$, and $\Lambda = 0.4\mu m$ covered with a Gr layer suggested by Zhao *et al.* [42] , (b) Absorptance with respect to the wavelength for RCWA code of the present paper and Zhao *et al.*'s paper.

6.4. Results and discussions for Gr-based structures

6.4.1. Spectrally selective emitter

As discussed earlier, Zhao *et al.* [42] showed that the structure in Figure 6.1(a) with $h = 0.2\mu m$, $b = 0.03\mu m$, and $\Lambda = 0.4mum$ exhibits a narrow band high absorptance. However, bonding the Gr having thickness of a fraction of a nm over the gaps between gratings is not practical. The structure shown in Figure 6.2(a) (Design 3) is proposed in the present study, in order to overcome to this issue. Instead of bonding the Gr layer over Ag grating, it can be coated over a Si film and the combined structure can be bonded over the Ag grating. It is observed that the thickness of the introduced silicon layer have a strong influence on the optical behavior of the proposed structures. Figure 6.4 shows the effect of the Si film thickness (t_{Si}) on the spectral absorptance. It can be observed that a strong absorption band can be achieved beyond $2\mu m$ around $t_{Si} = 0.327\mu m$ and $0.72\mu m$, with some absorption peaks at visible or near IR wavelengths. Moreover, the strong absorption band can be slightly tuned by changing the t_{Si}.

The spectral absorptance of the structure with $t_{Si} = 0.327\mu m$ (blue solid line) is presented in Figure 6.5. It can be observed that, the first absorptance peak is reduced from 100% at the wavelength $0.54\mu m$ to 75% at the wavelength $1.31\mu m$; however, the second peak is enhanced from 80% at the wavelength $1.5\mu m$ to 96% at the wavelength $2.58\mu m$ in comparison to the results of Zhao *et al.* [42] (red line). The observed enhancement is due to the coupling of the surface polaritons of the Si and Ag gratings. Next, the Gr layer is removed so that the Si layer is bonded on top of the Ag grating in order to understand the effect of the Gr layer on the considered structure. Figure 6.6 shows the spectral absorptance of both cases (with Gr and without Gr). While the Gr layer does not affect the absorptance peak at $2.58\mu m$, at $1.31\mu m$ the spectral absorptance increases by about 20%. Therefore, the effect of Gr layer varies with wavelength. The spectral absorptance of each part of the structure that is shown in Figure 6.2(a) is presented separately in Figure 6.7. It can be seen that, individual layers have a quite different behavior with respect to the whole structure when they are considered sepa-

rately. Specifically, the separated layers does not have significant absorptance at the wavelength of the absorption peaks ($\lambda = 2.58\mu m$). Therefore, the observed resonance is caused by the interaction between different layers.

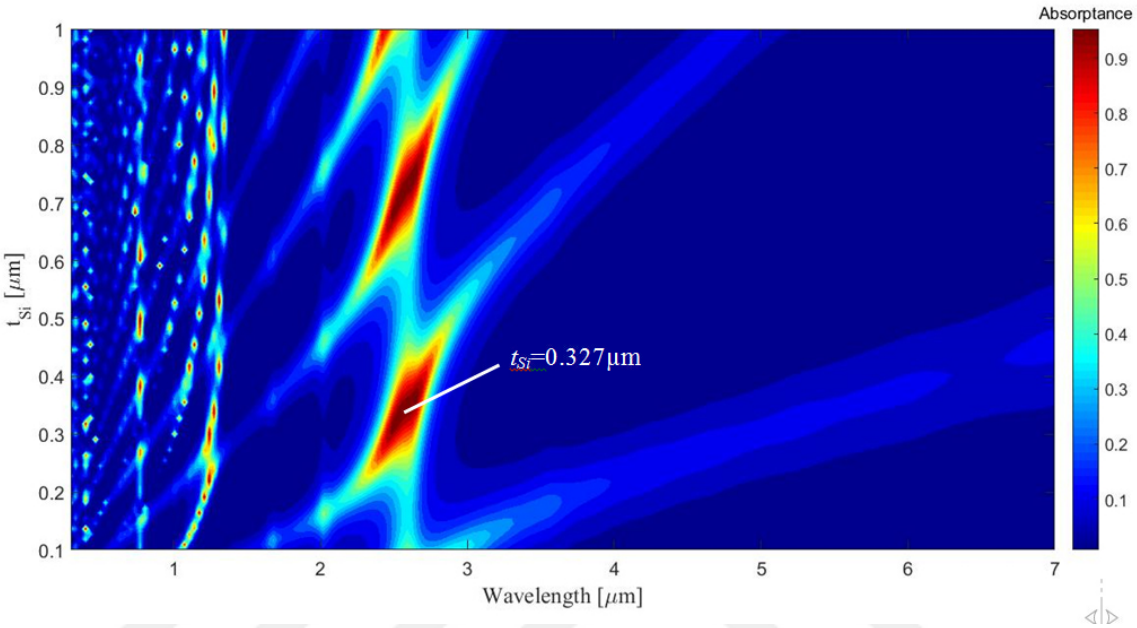


Figure 6.4. Absorptance contour plot showing the effect of Si film thickness (t_{Si}) with respect to the wavelength in Design 3 structure.

In order to observe the contribution of the each part of the structure, it is critical to specify where the radiation is absorbed. Power dissipation profile can be used to identify localized absorption, which can be calculated by the following equation [42]:

$$P_d(x,z) = \frac{1}{2}\varepsilon_0\omega\varepsilon''(x,z)|E(x,z)|^2 \tag{6.6}$$

where, ε'' is the imaginary part of the dielectric function, and E is the electric field. Figure 6.8 shows the power dissipation profile of the Design 1 structure at peak absorption wavelength of $2.58\mu m$ for without Gr and with Gr cases. As the figure illustrates, when the Gr is removed (Figure 6.8(a)) the grooves of the Ag grating have significant contribution on absorption due to the excitation of the magnetic polaritons inside the gratings narrow gaps [42]. As the Gr layer is added (Figure 6.8(b)), it plays a significant role on overall absorption. Accordingly, less radiation passes through the Gr

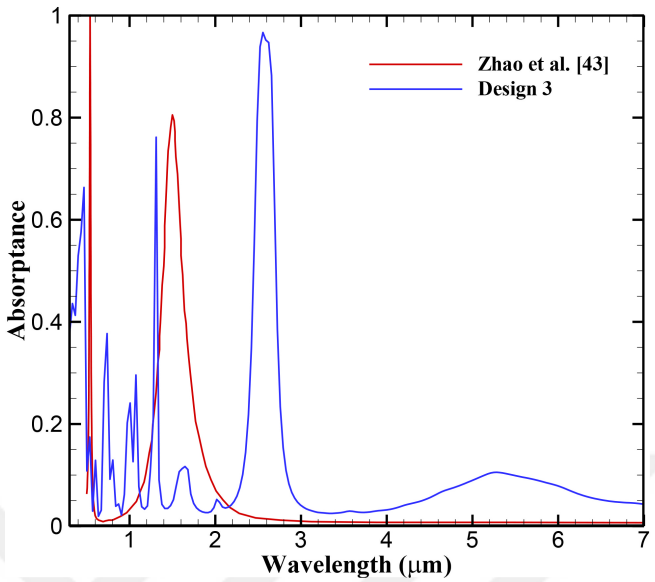


Figure 6.5. Absorptance spectrum of the structure shown in Design 3 (Figure 6.2(a)) and the structure introduced by Zhao *et al.* [42].

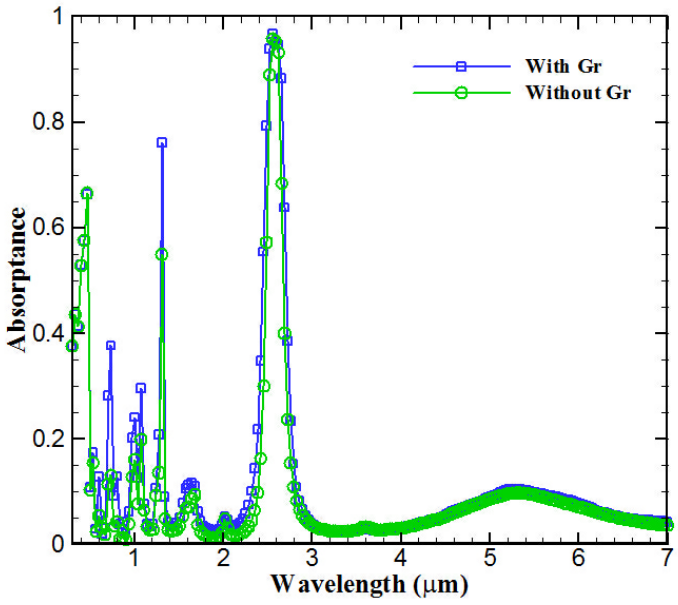


Figure 6.6. The effect of the Gr layer on absorptance of the Design 3 structure shown in Figure 6.2(a).

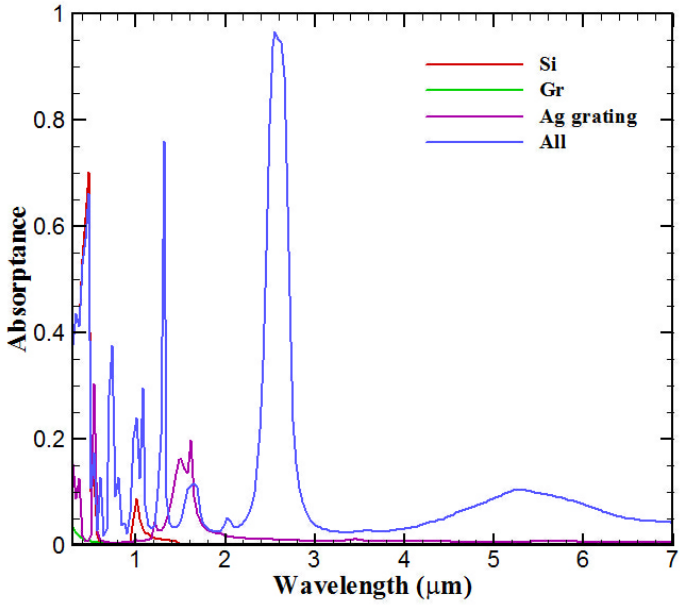


Figure 6.7. The absorptance spectrum of each separate layer of the Design 3 structure shown in Figure 6.2(a).

layer to reach the Ag grooves and it reduces the contribution of Ag grating on overall absorption. In order to see the power dissipation by Gr, the section indicated by the rectangular dashed line in Figure 6.8(b) is magnified in Figure 6.8(c) which shows the high absorption of the Gr layer.

Similar profiles are plotted for $1.31\mu m$, where second absorptance peak is observed, in Figure 6.9 for both with and without Gr cases. Similar to $2.58\mu m$ case, the absorption at $1.31\mu m$ is concentrated at the Gr layer once it is introduced. It can also be noted that, high absorption is observed at the corners of the Ag gratings and at this wavelength as the magnified image in Figure 6.9(c) shows, absorption by the Si layer is improved when the Gr layer is removed (Figure 6.9(a)).

The Design 4 structure shown in Figure 6.2(b) is investigated next. As the figure shows, Ag strips are considered. Gold could have been used in these structures, but our calculations suggest that, Ag could provide a better performance. Yet, in the long term, oxidation of the Ag may cause a reliability issue which needs a separate study.

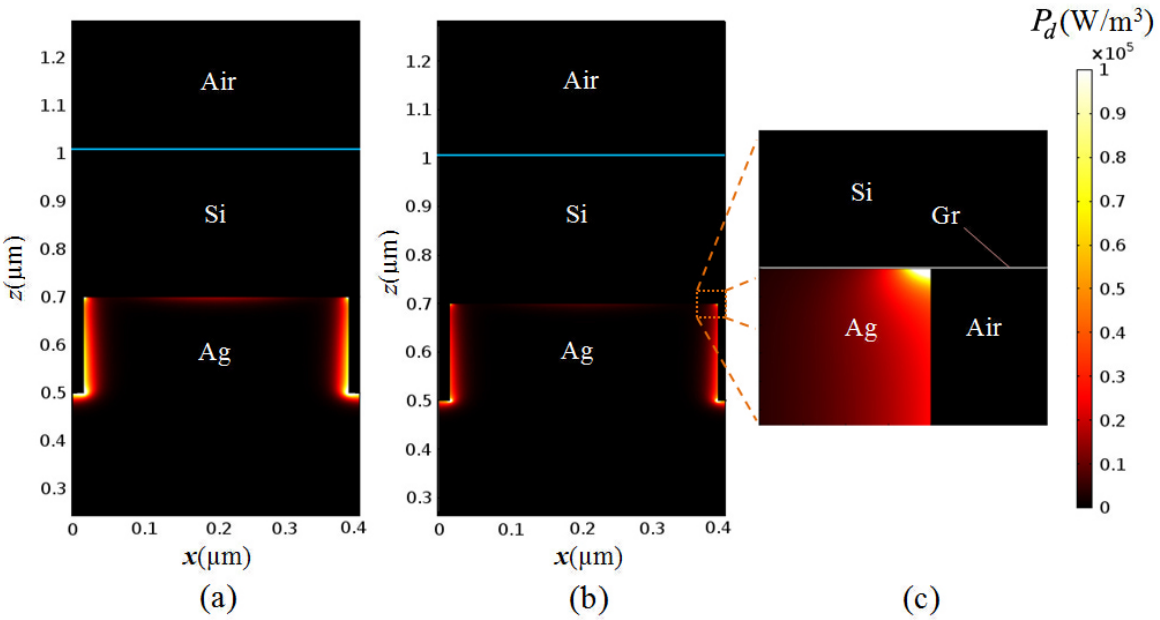


Figure 6.8. Power dissipation profile of the Design 3 structure at the wavelength of $2.58\mu m$ for without Gr (a) and with Gr (b) cases. The section indicated by the rectangular dashed line in (b) is magnified in (c).

The spectral absorptance of the structure with $h = 0.16\mu m$, $b = 0.007\mu m$, $\Lambda = 0.5\mu m$ is presented in Figure 6.10. It can be seen that a strong band absorptance of 85% is achieved at $1.78\mu m$, with relatively weaker absorbing bands at shorter wavelengths, with no absorption at larger wavelengths. Therefore, an approximately monochromatic absorptance can be obtained using this structure. Figure 6.11 compares the absorptance spectrum of the considered structure with a similar structure without the Gr layers. It can be seen that the absorptance of the peak point at wavelength of $1.78\mu m$ increases from 70% to 85% with the introduction of the Gr layers to the Ag strips. Therefore, the Ag strips play the main role on achieving the observed narrow-band absorptance and introducing the Gr layers only magnifies the absorptance at specific wavelengths. The resonance observed in Figure 6.10, for the structures with deep silver gratings having high aspect ratio (h/b) such as the structure presented in Figure 6.2(b) is due to the excitation of the magnetic polaritons inside the gratings narrow gaps which is caused by the strong coupling of the magnetic resonance inside the deep grating due to the incident electromagnetic waves [15]. Figure 6.12 shows the power dissipation

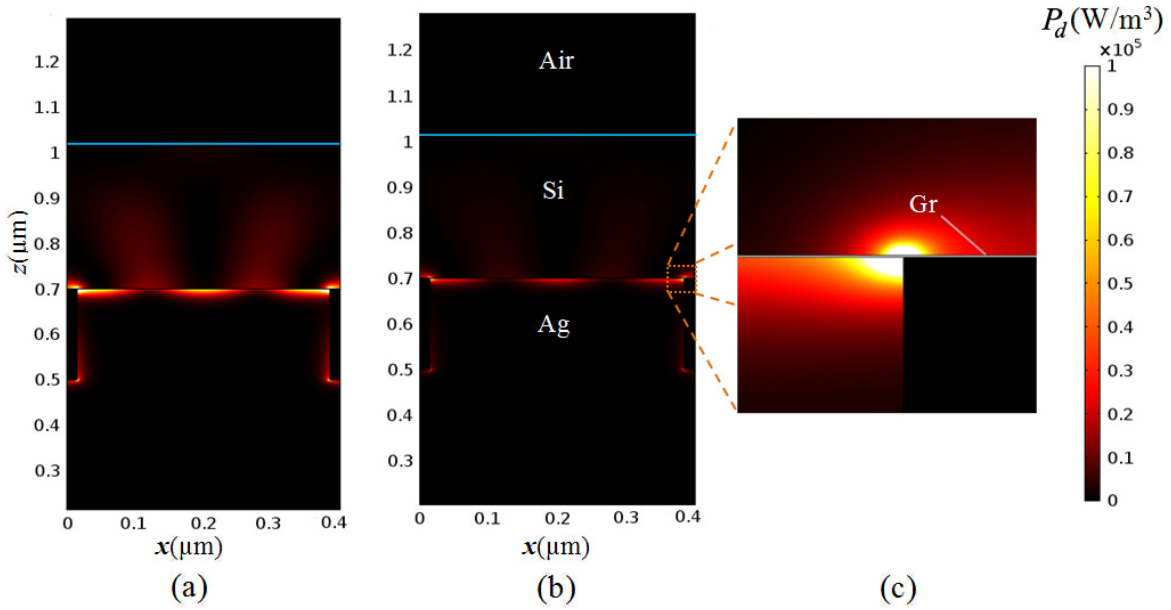


Figure 6.9. Power dissipation profile of the Design 3 structure at the wavelength of $1.31\mu m$ for without Gr (a) and with Gr (b) cases. The section indicated by the rectangular dashed line in (b) is magnified in (c).

profile of the structure. When there is no Gr in the structure (Figure 6.12(a)) only lower and side boundaries of the Ag strip absorbs. By introducing the Gr layers (Figure 6.12(b)), although the absorption of the Ag strip decreases slightly, Gr layers absorb significantly and increases the overall absorptance of the structure as shown in Figure 6.10. The indicated regions of the Figure 6.12(b) are magnified in Figure 6.12(c). As the figure shows, the major absorption of the top Gr layer is observed at the corner of the Ag strip. However, the bottom Gr layer has high absorption uniformly distributed along the layer. Therefore, the absorption enhancement due to Gr layers shown in Figure 6.10 is performed mostly by the bottom Gr layer.

6.4.2. Spectrally selective filter

It is shown that by changing the geometric parameters of the Design 4 structure, spectrally selective transmittance can be achieved. Figure 6.13 shows the transmittance spectrum of the structure in Figure 6.2(b) with $h = 0.29\mu m$, $b = 0.1\mu m$, and

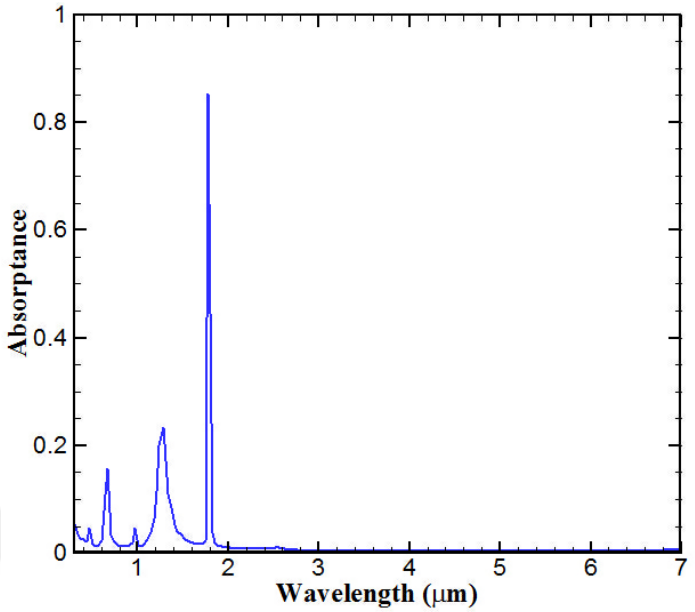


Figure 6.10. Absorptance spectrum of the Design 4 structure shown in Figure 6.2(b) with $h = 0.16\mu m$, $b = 0.007\mu m$, $\Lambda = 0.5\mu m$.

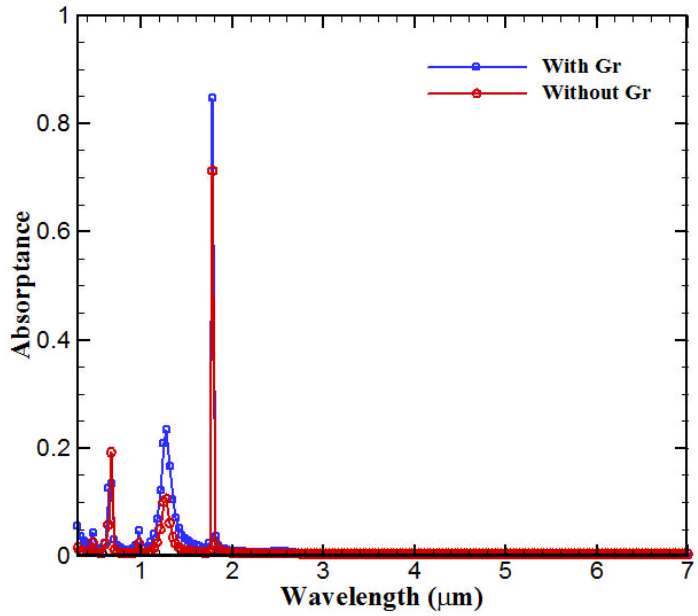


Figure 6.11. The effect of the Gr layer on absorptance of the Design 4 structure shown in Figure 6.2(b) with $h = 0.16\mu m$, $b = 0.007\mu m$, $\Lambda = 0.5\mu m$.

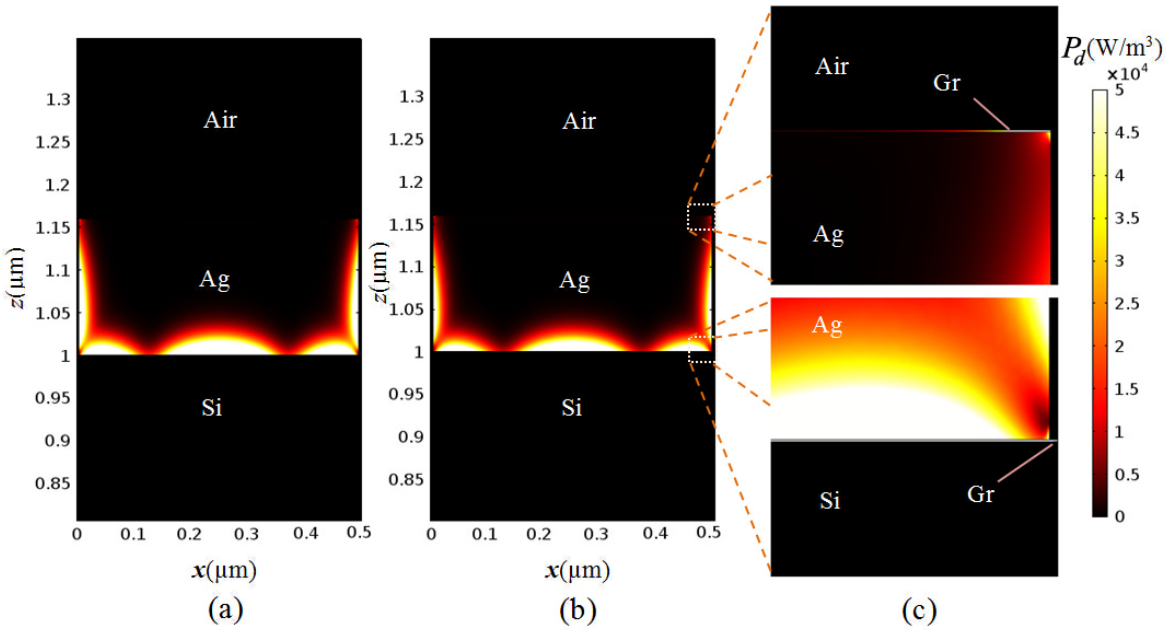


Figure 6.12. Power dissipation profile of the Design 4 structure at the peak absorptance wavelength ($1.78\mu m$) for without Gr (a) and with Gr (b) cases. The sections indicated by the rectangular dashed line in (b) are magnified in (c).

$\Lambda = 0.5\mu m$. According to the figure, high spectral transmittance, exceeding 80%, is observed between $1.07 - 1.78\mu m$ and following the cut-off wavelength, $1.78\mu m$, a monotonic increase in spectral transmittance is observed that reaches 50% around $7\mu m$. Therefore, this structure can be a good candidate as a filter for thermophotovoltaic (TPV) applications, where transmittance of convertible radiation is desired, if the transmitted radiation beyond the cut-off wavelength (green area) could have been filtered out as much as possible. In earlier chapters, we have suggested the use of Si/SiO_2 multilayered structures in [59] and combining these two concepts can further improve system efficiency. The combined filter proposed is presented in Figure 6.14. The thickness of the Si and SiO_2 layers can be calculated according to the quarter-wave theory as mentioned in [59].

For the structure shown in Figure 6.2(b) with spectral transmittance shown in Figure 6.14, the λ_1 can be chosen as $1.78\mu m$ to filter out the transmittance at longer wavelengths. Consequently, the thickness of the Si and SiO_2 layers are estimated as

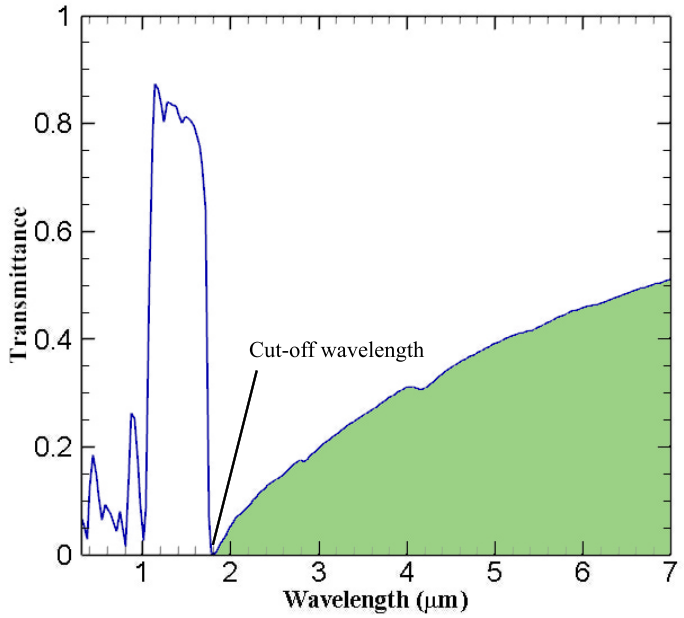


Figure 6.13. Transmittance spectrum of the Design 4 structure shown in Figure 6.2(b) with $h = 0.29\mu m$, $b = 0.1\mu m$, $\Lambda = 0.5\mu m$

$d_{Si} = 0.164\mu m$ and $d_{SiO_2} = 0.372\mu m$. The thickness of the first layer is considered as $d_{SiO_2}/2$ [59] in order to achieve anti-reflection effect as shown in Figure 6.14. Figure 6.15 presents the effect of gap distance (t_{gap}) on the transmittance of the entire structure. As the figure shows, the transmittance is highly dependent on the gap distance. The gap distance $0.725\mu m$ that is shown with white dashed line in Figure 6.15 has the maximum transmittance between $1.07 - 1.78\mu m$ of wavelength and the spectral transmittance of the structure with the considered gap is shown in Figure 6.16. As the figure shows, the transmittance at the wide band $1.78 - 3.1\mu m$ can be filtered using the Si/SiO_2 structure without significant change in the maximum transmittance between the range $1.07 - 1.78\mu m$. It was shown in [59] that cancelling out the transmittance in the wide range after cut-off wavelength has significant effect on the efficiency of the thermophotovoltaic systems' performance.

The introduced structure (Design 5) shown in Figure 6.14 is applied to a TPV system with GaSb cell with the band-gap wavelength of about $1.78\mu m$ which is changing with respect to the cell temperature obtained by Varshni equation (Equation (5.1)).

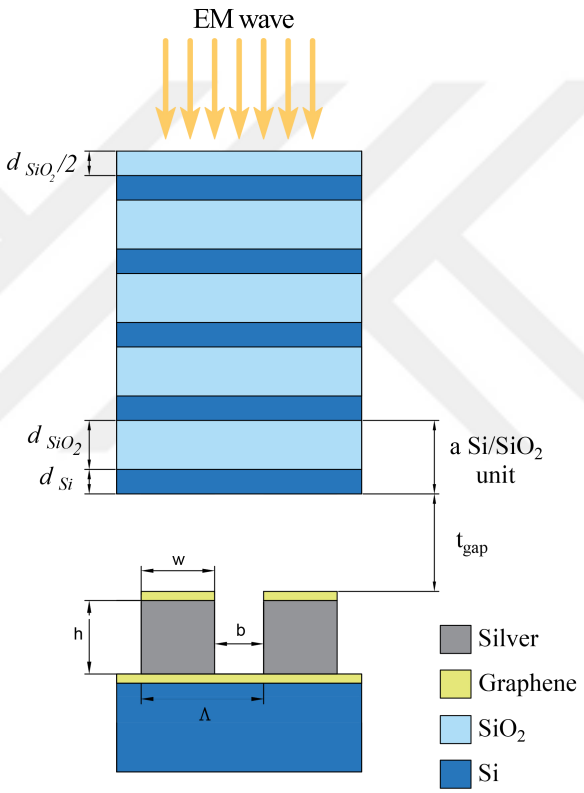


Figure 6.14. Considered structure in Figure 6.2(b) (Design 5) with Si/SiO_2 multilayered structure.

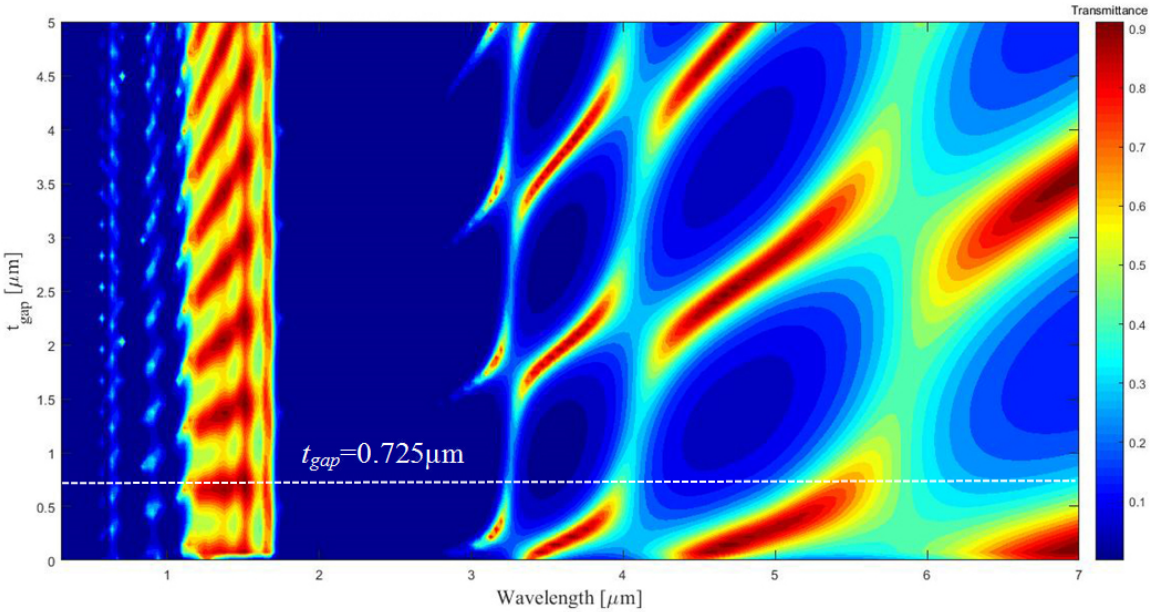


Figure 6.15. Transmittance spectrum of the Design 5 structure shown in Figure 6.14 for changing t_{gap}.

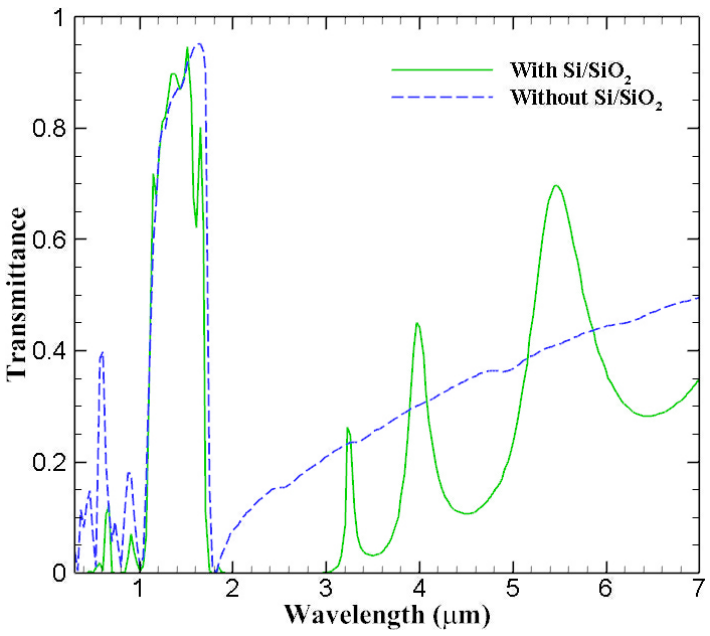


Figure 6.16. Transmittance spectrum comparison of the Design 4 structure shown in Figure 6.2(b) (blue dashed line) with the Design 5 structure shown in Figure 6.14 (green solid line).

The gap distance (t_{gap}) is optimized using Genetic algorithm (GA) global optimization method, where the TPV overall efficiency (Equation (4.1)) is considered as the fitness function. The optimized t_{gap} is found to be $0.719\mu m$.

The resulted overall efficiency of the proposed structure is compared with TPV systems with no filter, ideal filter, the filter introduced in the Figure 5.5(a) (Design 2) which is optimized for GaSb cell, and the Design 4 structure which is shown in Figure 6.17. As the figure shows, the overall efficiency of the Design 4 structure is similar to that of the Design 2 filter. However, by adding Si/SiO_2 multilayers (Design 5) the efficiency is enhanced about 15% for the emitter temperature of $1800K$. The enhancement is decreased as the emitter temperature drops. The efficiency enhancement can be attributed to two reasons: First, less heat is required to keep emitter at a specified temperature, since the filter reflects back the undesired longer wavelengths back to the emitter. Second, higher cell electrical conversion efficiency is achieved as a result of lower temperature in the cell.

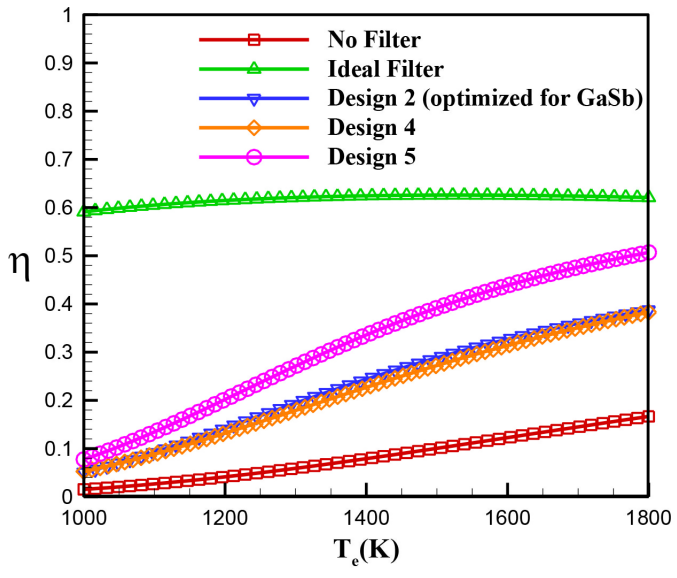


Figure 6.17. Overall efficiency of a GaSb based TPV cell with, no filter, ideal filter, the Design 2 filter, Design 4 filter, and Design 5 filter.

7. CONCLUSIONS AND RECOMMENDATIONS FOR FUTURE WORKS

7.1. Conclusions

As discussed, TPV devices can be considered as advantages tools to generate electrical energy from wasted heat in the industry. The TPV devices function based on same principles with the PV devices. However, instead of the solar energy, which is predominantly in the visible spectrum, TPV devices rely on infrared radiation from thermal sources to generate electricity. Small amount of energy can be produced by exposing a TPV cell directly in front of a thermal source, since the TPV cell can convert specific range of wavelength to the electricity and the rest of the spectrum will heat the cell resulting efficiency reduction. Therefore, using spectrally selective filters in the TPV devices are crucial.

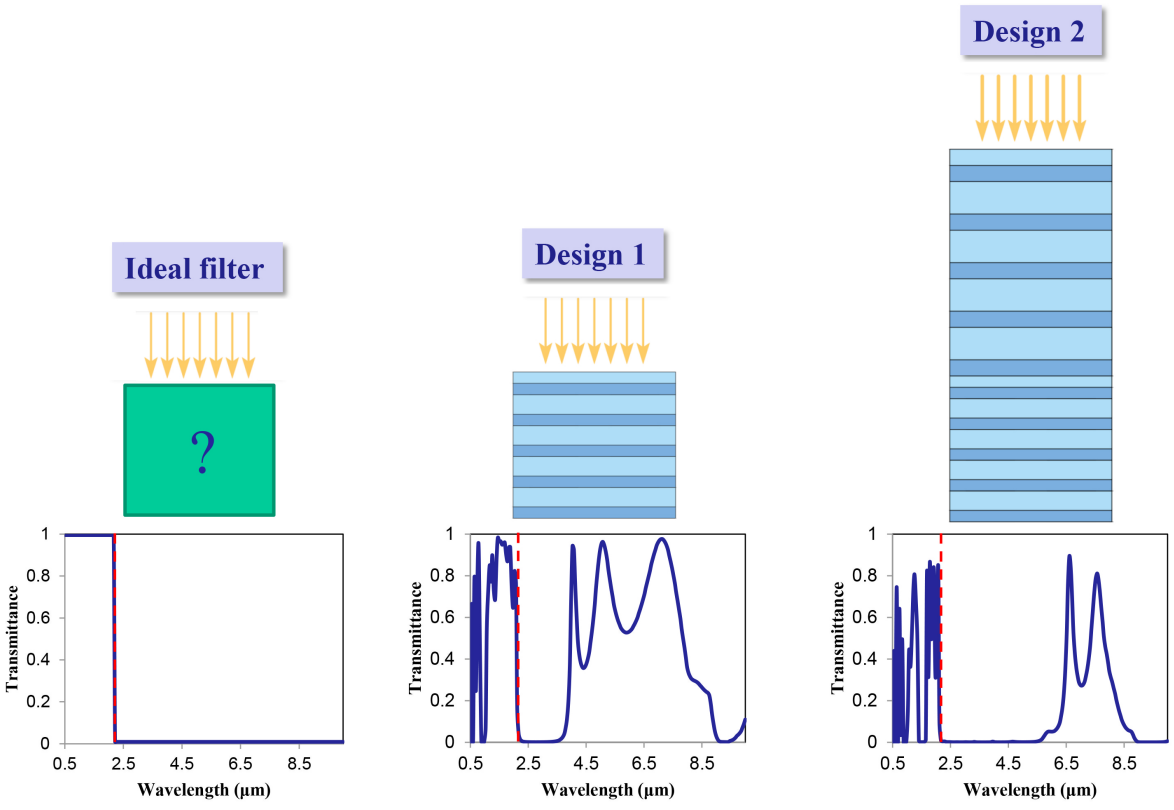


Figure 7.1. Considered cases in performance comparison for Si/SiO_2-based filters.

The present study focused on designing spectrally selective emitters/filters. An ideal filter in a TPV cell, transmits all the incoming radiation below the band-gap wavelength of the TPV cell and reflects the rest. In chapter 5 a filter is designed and optimized to meet the ideal filter as much as possible. The proposed structure composed of two sets of Si/SiO_2 1D multilayered units. In each set, the thicknesses of the Si and SiO_2 layers are assumed identical. However, in order to achieve anti-reflection effect in each set, the thickness of the first SiO_2 layer of each set has half a thickness of the SiO_2 layers at the rest of the related set. Transmittance of the filter is estimated by RCWA and a global optimization algorithm is used to find the best possible filter by considering the overall efficiency as an objective function. In addition to the outstanding spectrally selective behavior, since Si and SiO_2 are the materials that are widely used in diverse fields of nano-technology, the suggested 1D Si/SiO_2 multilayered structures can be manufactured precisely with low cost.

While the detailed design for InGaSb based TPV cell is presented, outcomes of designs for Si, GaSb, and $Ga_{0.78}In_{0.22}As_{0.19}Sb_{0.81}$ based cells also presented. The suggested structures shown in Figure 7.1 are compared with ideal filter. The results showed that, zero transmittance is achieved over a wide band above the band-gap wavelength by using the optimized structure. For an emitter temperature of $1800K$ the overall system efficiency, which is defined as electrical power output over input energy to the system, reaches 50% for InGaSb cell by using the optimized structure, where the efficiency of the system with ideal filter is 58%, and the efficiency of system without filter is approximately 25%. The small reduction in optimized filter's efficiency with respect to that of ideal filter is due to observed transmission in higher wavelengths. The results also showed that, for the considered emitter temperature range, Si type cell has the worst and $Ga_{0.78}In_{0.22}As_{0.19}Sb_{0.81}$ type cell has the best performance among the considered cell types.

In the last decade, Gr based structures are considered as efficient options to achieve spectrally selective structures due to its optical capabilities, which can be used in modulators, photodetectors, and TPV devices. In chapter 6 two graphene-based nano-structures are studied in order to explore their spectrally selective behavior. The

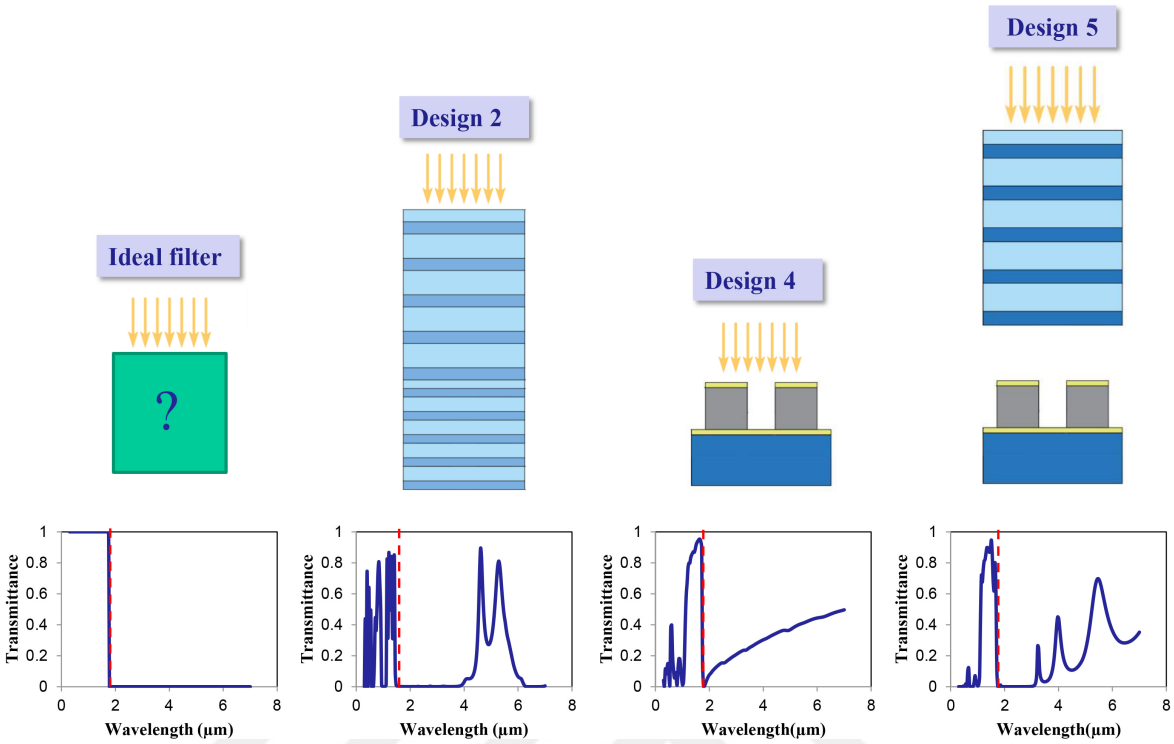


Figure 7.2. Considered cases in performance comparison for Gr-based filters.

results show that, narrow-band absorptance can be achieved. Specifically, for the Design 4 structure (Figure 6.2(b)) the absorptance occurs at almost a single wavelength. It is also shown that, by changing the geometric parameters of this structure, high transmittance is obtained at specific wavelength range, having sharp drop at the highest and lowest wavelengths of the range. The results showed that, adding Si/SiO_2 multilayered structure to the Design 4 structure shown in Figure 6.2(b) can enhance the spectral selectivity of the structure by canceling the transmittance on the wide wavelength range after cut-off wavelength which is crucial on enhancing the efficiency of the applications such as thermophotovoltaic devices. The suggested structure showed in Figure 6.14 is applied to a TPV system with GaSb cell. Figure 7.2 shows the cases that are considered to compare the performance of the suggested filter (Design 5). A good enhancement is seen on overall efficiency with respect to the Si/SiO_2 multilayered structure (Design 2) and Design 4.

In conclusion, in the present study, it is shown that using Si/SiO_2 multilayered filters can enhance the overall efficiency of a TPV system, since it reflects the major

portion of the unconvertible radiation emitted by a heat source back to the source and transmits the convertible portion to the cell. It is also shown that the Gr based structures can be a good candidate to achieve a spectrally selective filter/emitter to enhance the TPV system efficiency.

7.2. Future works

In this study it is shown that using Si/SiO_2 multilayered filters, a wide wavelength range can be banned and reflected back. This capability can be applied to different optical or thermal applications. The thicknesses of the layers can be optimized to achieve the desired spectrum. Radiative cooling can be considered as a potential application of these filters. Radiative cooling uses sky as a heat sink to cool the objects on Earth. The atmosphere is transparent for the wavelength range of $8-13\mu m$. However, the objects on the Earth emits at different wavelengths, which cannot passed the atmosphere. Using specific coatings or filters can help the objects to emit at the $8-13\mu m$ which will pass the atmosphere and cause the object to be cooled. by carefully selecting the thickness of the layers in Si/SiO_2 filters, the transparency at the desired wavelength range can be achieve.

It is shown that, Gr has a great potential to achieve monochromatic emission. This effect can be used in diverse applications such as sensors. However, achieving monochromatic emission in most of the wavelengths is still lacking in the literature. By examining different Gr based nano-structures such as Au gratings, W gratings, etc. emission wavelength can be tuned to diverse wavelengths.

Generally, TPV devices are used in the systems having relatively higher temperature thermal sources. Automobiles have different parts which are working at high temperatures. For example, in some sections of the exhaust system, the metal temperature can reach to $1000K$ and it is wasted by cooling systems or by exposing it to the flowing air. In some cases, several heat shields are used to prevent the possible damages of other parts caused by heat transferred from high temperature parts. Using TPV systems furnished on the shields can be advantages to utilize the great amount

of the wasted heat to generate electricity. Studying the feasibility of such systems and optimizing the filters according to the source temperature can be an interesting subject.

REFERENCES

1. Loster, M., "Total primary energy supply from sunlight", *Total Primary Energy Supply*, pp. 5–6, 2016.

2. Modest, M., *Radiative Heat Transfer*, ACADEMIC PRESS, California, USA, 2003.

3. Howell, J. R., R. Siegel and M. P. Menguc, *Thermal radiation heat transfer*, CRC PRESS, New York, NY, USA, 2010.

4. Francoeur, M., *Near-Field Radiative Transfer: Thermal Radiation, Thermophotovoltaic Power Generation And Optical Characterization*, Ph.D. Thesis, University of Kentucky, 2010.

5. O'Sullivan, F., I. Celanovic, N. Jovanovic, J. Kassakian, S. Akiyama and K. Wada, "Optical characteristics of one-dimensional Si/SiO2 photonic crystals for thermophotovoltaic applications", *Journal of Applied Physics*, Vol. 97, No. 3, p. 033529, 2005.

6. Mao, L. and H. Ye, "New development of one-dimensional Si/SiO2 photonic crystals filter for thermophotovoltaic applications", *Renewable Energy*, Vol. 35, No. 1, pp. 249–256, 2010.

7. GuangPing, L., X. YiMin, H. YuGe and L. Qiang, "Investigation of one-dimensional Si/SiO2 photonic crystals for thermophotovoltaic filter", *SCIENCE CHINA Technological Sciences*, Vol. 51, No. 11, p. 2031, 2008.

8. Mostafa, S. I., N. H. Rafat and S. A. El-Naggar, "One-dimensional metallic-dielectric (Ag/SiO2) photonic crystals filter for thermophotovoltaic applications", *Renewable Energy*, Vol. 45, No. Supplement C, pp. 245 – 250, 2012.

9. Wang, G., X. F. Cheng, P. Hu, Z. S. Chen, Y. Liu and L. Jia, "Theoretical analysis

of spectral selective transmission coatings for solar energy PV system", *International Journal of Thermophysics*, Vol. 34, pp. 2322–2333, 2013.

10. Sakr, E., Z. Zhou and P. Bermel, "Enhancing selectivity of infrared emitters through quality-factor matching", *SPIE Optical Engineering and Applications*, Vol. 9608, 2015.

11. Kocer, H., S. Butun, Z. Li and K. Aydin, "Reduced near-infrared absorption using ultra-thin lossy metals in Fabry-Perot cavities.", *Scientific reports*, Vol. 5, p. 8157, 2015.

12. Foley, J. J., C. Ungaro, K. Sun, M. C. Gupta and S. K. Gray, "Design of emitter structures based on resonant perfect absorption for thermophotovoltaic applications", *Optics Express*, Vol. 23, No. 24, pp. A1373–A1387, Nov 2015.

13. Sai, H., Y. Kanamori, K. Hane and H. Yugami, "Numerical study on spectral properties of tungsten one-dimensional surface-relief gratings for spectrally selective devices", *Journal of the Optical Society of America*, Vol. 22, No. 9, pp. 1805–1813, 2005.

14. Wan, J. T., "Tunable thermal emission at infrared frequencies via tungsten gratings", *Optics Communications*, Vol. 282, No. 8, pp. 1671–1675, 2009.

15. Zhao, B. and Z. M. Zhang, "Study of magnetic polaritons in deep gratings for thermal emission control", *Journal of Quantitative Spectroscopy and Radiative Transfer*, Vol. 135, No. Supplement C, pp. 81–89, 2014.

16. Nguyen-Huu, N., J. Pistora and M. Cada, "Wavelength-selective emitters with pyramid nanogratings enhanced by multiple resonance modes", *Nanotechnology*, Vol. 27, No. 15, p. 155402, 2016.

17. Wang, H., Y. Yang and L. Wang, "Wavelength-tunable infrared metamaterial by tailoring magnetic resonance condition with VO2 phase transition", *Journal of*

Applied Physics, Vol. 116, pp. 1–5, 2014.

18. Wang, H., Y. Yang and L. Wang, "Switchable wavelength-selective and diffuse metamaterial absorber/emitter with a phase transition spacer layer", *Applied Physics Letters*, Vol. 105, pp. 2012–2017, 2014.

19. Song, J., H. Wu, Q. Cheng and J. Zhao, "1D trilayer films grating with W/SiO2/W structure as a wavelength-selective emitter for thermophotovoltaic applications", *Journal of Quantitative Spectroscopy and Radiative Transfer*, Vol. 158, No. Supplement C, pp. 136 – 144, 2015, special Issue on the Second International Workshop on Micro-Nano Thermal Radiation.

20. Sai, H. and Y. Kanamori, "Spectrally selective thermal radiators and absorbers with periodic microstructured surface for high-temperature applications", *Microscale Thermophysical Engineering*, Vol. 7, pp. 101–115, 2003.

21. Sai, H., Y. Kanamori and H. Yugami, "High-temperature resistive surface grating for spectral control of thermal radiation", *Applied Physics Letters*, Vol. 82, p. 1685, 2003.

22. Sai, H., T. Kamikawa, Y. Kanamori and K. Hane, "Thermophotovoltaic generation with microstructured tungsten selective emitters", *AIP Conference Proceedings*, pp. 206–214, 2004.

23. Heinzel, A., V. Boerner, A. Gombert, B. Bläsi, V. Wittwer and J. Luther, "Radiation filters and emitters for the NIR based on periodically structured metal surfaces", *Journal of Modern Optics*, Vol. 47, No. 13, pp. 2399–2419, 2000.

24. Yeng, Y. X., J. B. Chou, V. Rinnerbauer, Y. Shen, S.-G. Kim, J. D. Joannopoulos, M. Soljacic and I. Celanovic, "Global optimization of omnidirectional wavelength selective emitters/absorbers based on dielectric-filled anti-reflection coated two-dimensional metallic photonic crystals", *Optics Express*, Vol. 22, pp. 21711–21718, 2014.

25. Chou, J. B., Y. X. Yeng, A. Lenert, V. Rinnerbauer, I. Celanovic, M. Soljačić, E. N. Wang and S.-G. Kim, "Design of wide-angle selective absorbers/emitters with dielectric filled metallic photonic crystals for energy applications", *Optics Express*, Vol. 22, No. S1, pp. A144–A154, Jan 2014.

26. Fang, X., C. Zhao and H. Bao, "Radiative behaviors of crystalline silicon nanowire and nanohole arrays for photovoltaic applications", *Journal of Quantitative Spectroscopy and Radiative Transfer*, Vol. 133, No. Supplement C, pp. 579 – 588, 2014.

27. Fang, X., M. Lou, H. Bao and C. Zhao, "Thin films with disordered nanohole patterns for solar radiation absorbers", *Journal of Quantitative Spectroscopy and Radiative Transfer*, Vol. 158, No. Supplement C, pp. 145 – 153, 2015, special Issue on the Second International Workshop on Micro-Nano Thermal Radiation.

28. Sai, H., H. Yugami, Y. Akiyama, Y. Kanamori and K. Hane, "Spectral control of thermal emission by periodic microstructured surfaces in the near-infrared region", *Journal of the Optical Society of America*, Vol. 18, No. 7, pp. 1471–1476.

29. Zhao, B., L. Wang, Y. Shuai and Z. M. Zhang, "Thermophotovoltaic emitters based on a two-dimensional grating/thin-film nanostructure", *International Journal of Heat and Mass Transfer*, Vol. 67, No. Supplement C, pp. 637 – 645, 2013.

30. Wang, H., V. P. Sivan, A. M. G. Rosengarten, P. Phelan and L. Wang, "Highly efficient selective metamaterial absorber for high-temperature solar thermal energy harvesting", *Solar Energy Materials and Solar Cells*, Vol. 137, pp. 235–242, 2015.

31. Yang, L., L. Mo, T. Chen, E. Forsberg and S. He, "A checkerboard selective absorber with excellent spectral selectivity", *Journal of Applied Physics*, Vol. 118, p. 183103, 2015.

32. Bonakdar, A., M. Rezaei, E. Dexheimer and H. Mohseni, "High-throughput realization of an infrared selective absorber/emitter by DUV microsphere projection lithography", *Nanotechnology*, Vol. 27, p. 035301, 2016.

33. Han, S. and B. J. Lee, "Control of thermal radiative properties using two-dimensional complex gratings", *International Journal of Heat and Mass Transfer*, Vol. 84, No. Supplement C, pp. 713 – 721, 2015.

34. Lee, B. J., Y.-B. Chen, S. Han, F.-C. Chiu and H. J. Lee, "Wavelength-Selective Solar Thermal Absorber With Two-Dimensional Nickel Gratings", *Journal of Heat Transfer*, Vol. 136, p. 072702, 2014.

35. Ogawa, S., D. Fujisawa, H. Hata, M. Uetsuki, K. Misaki and M. Kimata, "Mushroom plasmonic metamaterial infrared absorbers", *Applied Physics Letters*, Vol. 106, pp. 1–5, 2015.

36. Stelmakh, V., W. R. Chan, J. D. Joannopoulos, M. Soljacic and I. Celanovic, "Sputtered tantalum photonic crystal coatings for high-temperature energy conversion applications", pp. 1134–1137, 2015.

37. Butun, S. and K. Aydin, "Structurally tunable resonant absorption bands in ultrathin broadband plasmonic absorbers", *Optics Express*, Vol. 22, No. 16, pp. 19457–19468.

38. Woolf, D., J. Hensley, J. G. Cederberg, D. T. Bethke, A. D. Grine and E. A. Shaner, "Heterogeneous metasurface for high temperature selective emission", *Applied Physics Letters*, Vol. 105, p. 8, 2014.

39. Kocer, H., S. Butun, B. Banar, K. Wang, S. Tongay, J. Wu and K. Aydin, "Thermal tuning of infrared resonant absorbers based on hybrid gold-VO2 nanostructures", *Applied Physics Letters*, Vol. 106, 2015.

40. Ye, H., H. Wang and Q. Cai, "Two-dimensional VO2 photonic crystal selective emitter", *Journal of Quantitative Spectroscopy and Radiative Transfer*, Vol. 158, No. Supplement C, pp. 119 – 126, 2015, special Issue on the Second International Workshop on Micro-Nano Thermal Radiation.

41. Liu, X. L., B. Zhao and Z. M. Zhang, "Blocking-assisted infrared transmission of subwavelength metallic gratings by graphene", *Journal of Optics*, Vol. 17, No. 3, p. 035004, 2015.

42. Zhao, B., J. M. Zhao and Z. M. Zhang, "Enhancement of near-infrared absorption in graphene with metal gratings", *Applied Physics Letters*, Vol. 105, p. 031905, 2014.

43. Lu, H., B. P. Cumming and M. Gu, "Highly efficient plasmonic enhancement of graphene absorption at telecommunication wavelengths", *Optics Letters*, Vol. 40, No. 15, pp. 3647–3650, 2015.

44. Zhan, T. R., F. Y. Zhao, X. H. Hu, X. H.Liu and J. Zi, "Band structure of plasmons and optical absorption enhancement in graphene on subwavelength dielectric gratings at infrared frequencies", *Physical Review B*, Vol. 86, p. 165416, 2012.

45. Liu, J.-T., N.-H. Liu, J. Li, X. J. Li and J.-H. Huang, "Enhanced absorption of graphene with one-dimensional photonic crystal", *Applied Physics Letters*, Vol. 101, p. 052104, 2012.

46. Alaee, R., M. Farhat, C. Rockstuhl and F. Lederer, "A perfect absorber made of a graphene micro-ribbon metamaterial", *Optics Express*, Vol. 20, No. 27, pp. 28017–28024, 2012.

47. Thongrattanasiri, S., F. H. L. Koppens and F. J. G. de Abajo, "Complete optical absorption in periodically patterned graphene", *Physical Review Letters*, Vol. 108, p. 047401, 2012.

48. RUMPF, R. C., *Design and optimization of nano-optical elements by coupling fabrication to optical behavior*, Ph.D. Thesis, University of Central Florida, 2006.

49. Zhao, B. and Z. M. Zhang, "Study of magnetic polaritons in deep gratings for thermal emission control", *Journal of Quantitative Spectroscopy and Radiative Trans-*

fer, Vol. 135, No. Supplement C, pp. 81 – 89, 2014.

50. Mokkapati, S. and K. R. Catchpole, "Nanophotonic light trapping in solar cells", *Journal of Applied Physics*, Vol. 112, p. 101101, 2012.

51. Li, L., "Use of Fourier series in the analysis of discontinuous periodic structures", *Journal of the Optical Society of America*, Vol. 13, No. 9, pp. 1870–1876, 1996.

52. Lyndin, N. M., O. Parriaux and A. V. Tishchenko, "Modal analysis and suppression of the Fourier modal method instabilities in highly conductive gratings", *Journal of the Optical Society of America*, Vol. 24, No. 12, pp. 3781–3788, 2007.

53. Moharam, M. G., T. K. Gaylord, E. B. Grann and D. A. Pommet, "Formulation for stable and efficient implementation of the rigorous coupled-wave analysis of binary gratings", *Journal of the Optical Society of America*, Vol. 12, No. 5, pp. 1068–1076, 1995.

54. Moharam, M. G., T. K. Gaylord, D. A. Pommet and E. B. Grann, "Stable implementation of the rigorous coupled-wave analysis for surface-relief gratings: enhanced transmittance matrix approach", *Journal of the Optical Society of America*, Vol. 12, No. 5, pp. 1077–1086, 1995.

55. Zhai, X., J. Lai, H. Liang and S. Chen, "Performance analysis of thermophotovoltaic system with an equivalent cut-off blackbody emitter", *Journal of Applied Physics*, Vol. 108, p. 074507, 2010.

56. Queisser, H. J., "Detailed balance limit for solar cell efficiency", *Materials Science and Engineering: B*, Vol. 159, No. Supplement C, pp. 322 – 328, 2009.

57. Dupré, O., R. Vaillon and M. Green, "Physics of the temperature coefficients of solar cells", *Solar Energy Materials and Solar Cells*, Vol. 140, No. Supplement C, pp. 92 – 100, 2015.

58. Melanie, M., *An introduction to genetic algorithms*, A Bradford Book The MIT Press, Massachusetts, USA, 1999.

59. Khosroshahi, F. K., H. Ertürk and M. P. Mengüç, "Optimization of spectrally selective Si/SiO2 based filters for thermophotovoltaic devices", *Journal of Quantitative Spectroscopy and Radiative Transfer*, Vol. 197, No. Supplement C, pp. 123 – 131, 2017, the Eight International Symposium on Radiative Transfer.

60. Lide, D. R. and W. M. Haynes, *Handbook of Chemistry and Physics*, CRC Press, Florida, USA, 2010.

61. Francoeur, M., R. Vaillon and M. P. Menguc, "Thermal impacts on the performance of nanoscale-gap thermophotovoltaic power generators", *IEEE Transactions on Energy Conversion*, Vol. 26, No. 2, pp. 686–698, 2011.

62. Wolpert, D. and P. Ampadu, *Managing temperature effects in nanoscale adaptive systems*, Springer, Mainz, Germany, 2012.

63. Wang, H. and L. Wang, "Perfect selective metamaterial solar absorbers", *Optics Express*, Vol. 21, No. S6, pp. A1078–A1093, 2013.